LA-UR -81-1270

TITLE: PHERMEX Applications to Study High-Pressure Flow and Detonation Waves

AUTHOR(S): Richard D. Dick

MASTER

SUBMITTED TO: 1st European Conference on Cineradiography with Photons or Particles

University of California

LOS ALAMOS SCIENTIFIC LABORATORY
Post Office Box 1663 Los Alamos, New Mexico 87545
An Affirmative Action/Equal Opportunity Employer

Form No. 836 R3
St. No. 2629
9/78

UNITED STATES
DEPARTMENT OF ENERGY
CONTRACT W-7405-ENG. 36

PHERMEX Applications to Study High-Pressure Flow and Detonation Waves[a]

Richard D. Dick
Los Alamos National Laboratory
Box 1663, MS-942
Los Alamos, NM 87545

ABSTRACT

PHERMEX, an acronym for Pulsed High-Energy Radiographic Machine Emitting X Rays, has been used as a diagnostic tool to make quantitative measurements from radiographs of inert materials under dynamic high-pressure conditions and of explosives during the detonation process.

In some experiments, radiography is the best method (compared to high-speed optical cameras and contactor pins) to study complicated hydrodynamic flow occurring in a dynamic experiment. To demonstrate the versatility and uniqueness of PHERMEX and the radiographic method, several experiments on inert solids having high and low atomic numbers will be discussed with some particulars. This includes the observation of the 11.0-GPa-pressure phase transition for antimony and the accompanying two-shock structure and the off-Hugoniot data for lead using regular reflection. Also, by careful design of a radiographic experiment, the Hugoniot state behind a shock front can be completely and precisely specified. Aluminum is an example of a material studies in this manner.

PHERMEX is useful in studying some detonation properties of explosives. As an illustration, the discussion will include radiographic results of divergence characteristics of a detonation wave in sensitive and insensitive explosives as it propagates past a corner and the effect of preshocking on the detonation process of insensitive explosives when the detonation wave interacts with a region that has been shock-compressed at a pressure too low to cause detonation.

The above are only a few of the hundreds of radiographic studies of shock-wave phenomena of solids and detonation characteristics of explosives. A complete list of PHERMEX experiments is published in "LASL PHERMEX Data Volumes, I, II, and III," University of California Press, Berkeley and Los Angeles, California, 1980, C. L. Mader Editor.

[a]Work performed under the auspices of the U.S. Department of Energy

PHERMEX, an acronym for Pulsed High-Energy Radiographic Machine Emitting X rays, has been used in multiple-experiment flash radiography to study various hydrodynamic phenomena. Since PHERMEX became operational in 1963, many dynamic high-pressure experiments[1] have been performed on many different inert and reactive materials that have low and high atomic numbers and densities. In this paper, only a few of the many experiments are discussed.

The subjects for the first section are single-shock Hugoniot data for aluminum[2] using perpendicular drive, off-Hugoniot data on aluminum[3,4] using reflected rarefaction and Mach-reflection techniques, high-pressure Hugoniot experiments on lead[5] using regular-reflection methods, and the results of studies to observe the presence of double shock waves in several solids[6]. The second section is a discussion of experiments to examine the corner-turning properties of sensitive and insensitive[7] explosives. In these studies, PHERMEX radiographs provided unique information about the divergence of a detonation wave as it propagates past a 90° corner. In the third section, radiographic experiments are described in which desensitizing action of heterogeneous explosives was accomplished by preshocking techniques. The results of these experiments have been numerically modeled[8] using the "Forest Fire" technique.[9]

A. DYNAMIC EXPERIMENTS ON INERT MATERIALS

Single-shock Hugoniot data can be obtained from flash radiographs of explosive-metal systems using x-ray sources that have very good spatial and time-resolution characteristics. Using radiographic techniques for measuring equation-of-state properties requires that small differences in areal density be observable, that edges and discontinuities be distinguishable, and that sufficient flux and penetrating radiation be available to accurately measure angles, interface positions, and slight material density changes. The use of PHERMEX on carefully designed experiments has produced very good data from Mach-reflection, regular-reflection, and oblique-drive techniques on many different materials.

Hugoniot data on aluminum were obtained by means of a detonation wave proceeding at right angles to the aluminum interface. A schematic of the fluid dynamics is shown in Fig. 1. Since the detonation velocity (D) is assumed to be constant, the shock velocity (U_s) in the aluminum is given by

$$U_s = D \sin\theta \quad .$$

For the single-shock condition, the particle velocity (U_p) and the interface deflection are related by

$$U_p = \frac{D \tan\theta}{\cos\theta + \sin\theta \tan\alpha} \quad .$$

The pressure in the aluminum is calculated from

$$P = \rho_0 U_s U_p$$

where ρ_0 is the initial density. By using different explosives and hence different detonation velocities, Hugoniot points can be obtained. It is very important to choose well characterized explosives and that the detonation front be planar and at right angles to the interface. Figure 2 is a reproduction of a static radiograph of a typical perpendicular-drive experiment on aluminum. The assembly consisted of a block of explosive [illegible]

by 100 mm by 127 mm long in contact with the aluminum sample that was 64 mm wide, 100 mm thick, and 114 mm long. The radiographic thickness was 100 mm. A plane-wave explosive lens initiated the driving explosive from below. The dynamic radiograph shown in Fig. 3 was taken after the detonation wave had traveled about 75 mm. Figure 4 is a line drawing showing the principal features on the radiograph. Line OA is the detonation wave, OB the shock wave, and OC the interface. Angles θ and α were measured at the intersection point O because the shock and interface were both curved. The results from three experiments on aluminum using TNT, Composition B-3, and PBX-9404 explosives are plotted in the U_s-U_p plane shown in Fig. 5 and listed in the table of Fig. 6. The U_s-U_p data obtained radiographically agrees very well with the well-known Hugoniot curve[10] for aluminum. This technique was used to obtain Hugoniot data for other materials[2].

In addition to obtaining Hugoniot data on the sample materials from these experiments, some properties of the driving explosive can be determined also. Once the angle α and the pressure in the sample is determined, the Chapman-Jouget (C-J) pressure of the explosive can be calculated[11] from a gamma-law equation of state of the form

$$E = \frac{P}{\rho(\gamma - 1)} - Q \quad .$$

E and ρ are the energy and density behind the detonation front, γ is a constant for the explosive, P is the C-J pressure, and Q is the energy release from the detonation reaction. The calculational procedure is to choose a value for gamma that matches the measured pressure in the sample and the angle α, given the detonation velocity and initial density of the explosive.

Off-Hugoniot data for a sample can be obtained by reflecting a shock wave from a second material with a different impedance. In this experimental situation, either a reflected shock or a reflected rarefaction will be formed depending on whether the impedance is larger or smaller than the sample. Figure 7 is a schematic drawing of the oblique-reflection technique. This technique[3] was used to measure the sound speed in preshocked aluminum. In this case, the reflected wave is a rarefaction wave, and measurement of angle β is a function of the sound speed as it travels into the preshocked aluminum. The experiment consisted of placing two 203-mm-long by 102-mm-square blocks of Composition B-3 explosive on two sides of an aluminum wedge machined to have two 40° angles. Two plane-wave explosive lenses initiated the explosive block simultaneously. Tantalum foils were embedded in the aluminum for radiographic contrast. Figure 8 is a reproduction of the static radiograph of the sound- speed experiment. A reproduction of the dynamic radiograph is shown in Fig. 9, and a line drawing of the main features is shown in Fig. 10.

At the aluminum wedge-air interface, the two incident shock waves strike the interface obliquely causing a rarefaction wave to be reflected back into the recompressed aluminum. By measuring β and θ at the point of contact and by knowing the induced pressure in the aluminum, the speed (C_p) of the rarefaction wave in the preshocked aluminum can be calculated from the expression

$$C_p = U_p \cos(\beta + \theta) + U_s \sin\beta / \sin\theta \quad .$$

The results from the aluminum experiment are U_s = 7.22 km/s, U_p = 1.40 km/s, θ = 40°, β = 40.2°, C_p = 7.49 km/s, P = 27.4 GPa, and ρ = 1.21. Subscript "p" indicates that the measurement is behind the reflected shock

wave. Measurement of the angles β and θ must be made at the intersection point formed by the principal shock and the rarefaction wave at the interface because of curvature.

Reflected oblique shock-wave experiments for which the collision was symmetric ($\delta = 0$ in Fig. 7) have been performed on lead using PHERMEX. The regular-reflection experiment described here consisted of a 14.0-mm-wide by 25.4-mm-thick by 127.0-mm-long lead sample sandwiched between two pieces of PBX-9404, each 63.5 mm wide by 25.4 mm thick by 127.0 mm long. A P-081 plane-wave explosive lens initiated the PBX-9404. A reproduction of the dynamic radiograph is shown in Fig. 11. By measuring the angles β and θ (see Fig. 7) and knowing the incident shock state, the reflected shock and particle velocities (U_{sr} and U_{pr}) can be determined from the following expressions

$$U_{pr} \cos \beta = U_p \cos \theta$$

and

$$U_{sr} = U_p \cos (\beta + \theta) + U_s \sin \beta / \sin \theta \quad .$$

Results from the lead experiment follow: $U_s = 2.911$ km/s, $U_p = 0.601$ km/s, $P = 19.8$ GPa, $\theta = 19.32^{\circ}$, $\beta = 21.16^{\circ}$, $U_{sr} = 3.634$ km/s, $U_{pr} = 0.608$ km/s, and $P_r = 51.4$ GPa. From these results, the Grüneisen ratio (Γ) was calculated to be 1.96.

PHERMEX radiographs clearly show the formation of both the first and second waves in materials shocked to a pressure near the phase transition. The pressure associated with the first wave is the pressure of the transition and the second wave corresponds to the overdriving pressure. Perpendicular-drive techniques, previously discussed, were used to perform radiographic experiments on bismuth and antimony, both solids, and on carbon disulfide, a liquid. The experiments consisted of blocks of explosive initiated by a P-040 lens in contact with the solid samples. A reproduction of a static radiograph of a typical arrangement is shown in Fig. 12. The two-shock structure observed in bismuth is shown in Fig. 13, and Fig. 14 is a line drawing showing the principal features. An analysis of the radiographs indicate that the first- and second-shock curves originate from the same point on the interface, and hence, the transition time is postulated to be essentially instantaneous. A measurement of the angles subtended by the two shock waves and knowing the detonation velocity of the baratol explosive yields a transition pressure of about 2.7 GPa. This value is in good agreement with previous work[12,13] using different diagnostic methods. In contrast, the transformation[14] in antimony at about 11.0 GPa does not occur instantaneously but requires 2-3 μs. Figure 15 is a reproduction of the dynamic radiograph of a two-shock experiment on antimony, and Fig. 16 is a line drawing of the main features. From the radiograph, the first shock wave has a downward curvature (from a decreasing velocity), while the second wave originates at the same point as the first wave but starts at a very low velocity (small slope) and then accelerates to a higher terminal velocity. If the second wave is extrapolated back to the antimony-baratol interface, a time delay of 2-3 μs is obtained agreeing with Warnes'[14] observations.

The final example of a two-shock structure associated with a phase change is an experiment in which a block of Composition B-3 explosive drives liquid carbon disulfide at right angles. A phase transition[15,16] occurs in carbon disulfide at about 6.0 GPa, but the question about the presence of a

two-shock wave structure associated with the transition has remained unanswered. A radiographic experiment was conducted recently to answer this question. Figure 17 is a reproduction of the dynamic radiograph from the carbon disulfide experiment. A double-shock structure was observed. The transition pressure of 6.8 GPa was calculated from a measurement of θ (26.2^{o}) for the first shock wave, from the knowledge of the detonation velocity of the Composition B-3 explosive (D = 7.93 km/s), and the carbon disulfide equation of state.

Both liquid and solids exhibit a two-shock structure when shocked to a pressure at which a significant phase transistion occurs.

B. DIVERGENCE STUDIES ON DETONATION WAVES IN SENSITIVE AND INSENSITIVE EXPLOSIVES

An important property of an explosive in practical applications is the ability of the detonation wave to turn a corner and propagate unabated. A series of flash-radiographic experiments using PHERMEX has been performed to compare the ability of the insensitive explosives X-0219, X-0291, and PBX-9502, and the sensitive explosive PBX-9501 to turn a corner with a 90^{o} angle. Each of these explosives is described in Fig. 18.

Figure 19 is a diagram of a typical explosives assembly, and Fig. 20 illustrates the radiographic geometry used at PHERMEX. A reproduction of a typical static radiograph is shown in Fig. 21. The explosive charge as shown in the figures was L-shaped with a 90^{o} inside corner and presented a radiographic thickness of 146 mm. A Lucite plate cemented to the explosive served as a mechanical support and as a means to determine some of the explosive's parameters. The insensitive explosive was detonated by a P-081 lens and a PBX-9501 booster explosive. Only the P-081 lens was used to initiate the PBX-9501 samples. The dynamic radiographs were taken at different times to observe the progress of the detonation wave after propagating beyond the corner.

The results on the insensitive explosives X-0219, X-0291, and PBX-9502 will be described in this paragraph. Figures 22-24 are dynamic radiographs in succeeding time steps of corner turning in X-0219, the most insensitive of the explosives. The distinguishing features of the radiographs are the curved and well-defined detonation front in the explosive, the large triangular-shaped zone of high-density material near the corner, the sharply defined boundary between the compressed zone and the explosive gases, the well-defined shock wave in Lucite, and the slanted front and back surfaces of the Lucite plate. Figures 25-27 are dynamic radiographs of corner turning in X-0291 which is more sensitive than X-0219. The features on the radiographs are similar to X-0219 except that the size of the compressed region at the corner is smaller. Reproductions of dynamic radiographs of PBX-9502 are shown in Figs. 28-30. The principal features on the radiographs are similar to X-0219 and X-0291. The compressed zone is very much smaller than observed for X-0219. For comparison, the corner-turning characteristics for the sensitive PBX-9501 are shown in the dynamic radiographs of Figs. 31-33. The features are very similar to the insensitive explosives except there was no compressed zone at the corner and the detonation wave appears to be spreading past the corner with a circular shape whose center was at the corner.

By way of explanation, it appears that as the detonation front in the insensitive explosives propagates past the right-angle corner, a compressed and unreacted zone begins to take shape from a decrease in pressure. This zone builds to a size and shape that depends on the sensitivity of the explosive, that is, for a sensitive explosive like PBX-9501 there is no

unreacted zone, but for an insensitive explosive like X-0219, there is a very large unreacted region. Larger ratios of TATB explosive to binder as in X-0291 and PBX-9502 have correspondingly smaller unreacted zones. The composite drawings of the radiographic features for X-0219 and PBX-9502 are shown in Figs. 34 and 35. These illustrate that the detonation front, originally at the apex of the compressed zone, travels down the side of the zone eventually leaving the region isolated within the explosive gases. This zone appears to persist for many microseconds and it may never detonate in the normal sense. The arrows in Figs. 34 and 35 signify a decreasing detonation velocity which suggests a decrease in detonation pressure after the front turns through about a 45° angle.

From measurements of the angles θ and α from the radiographs and a knowledge of the detonation velocities of X-0219 (7.53 km/s) and PBX-9502 (7.63 km/s) and the equation of state of Lucite, the C-J pressure (P_{CJ}) and the gamma-value of the explosive can be calculated from the gamma-law formulation of the detonation. The computed values for gamma and P_{CJ} and other parameters are compared to those of other explosives in Fig. 36.

The results from the corner-turning experiments are summarized in Fig. 37.

C. PRESHOCKED BARATOL, PBX-9502, AND X-0219 EXPLOSIVES

PHERMEX was used to study the behavior of a detonation wave proceeding into preshocked explosive. The sample explosives under study were baratol, PBX-9502, and X-0219 and are described in Fig. 18. The experimental concept was for a detonation wave to interact with a shock wave produced by the impact of a steel plate with the explosive and directed at a right angle to the detonation front. The characteristics of the interaction of the detonation with preshocked explosive depends on the shock pressure which in turn governs the run-to-detonation distance. In each experiment, the sample size was 65 mm by 100 mm by 150 mm with the radiographic thickness being 100 mm.

In the baratol experiment, a 6.0-mm-thick steel plate was launched by a 12.7-mm-thick slab of Detasheet explosive to a velocity of 0.88 km/s after a run of 25.0 mm. Figure 38 is a schematic of the experiment, and Fig. 39 is a reproduction of the static radiograph taken by PHERMEX. Following plate impact, the induced shock wave, which had an amplitude of 7.0 GPa, converts to a detonation wave after propagating a distance of about 20 mm. The two detonation waves in baratol then interact forming a Mach stem. Figure 40 is a reproduction of the dynamic radiograph taken about 10 μs after the two waves had intersected. The baratol flow problem, shown in Fig. 41, was modeled[8] using a two-dimensional reactive Lagrangian code and the Forest Fire[9] reaction rate.

The experiment using X-0219 as the sample explosive was like the baratol test in all respects. Figure 42 is a reproduction of the dynamic radiograph. At the input shock pressure of about 5.5 GPa produced by plate impact in this experiment, the shock wave must run about 150 mm before transforming to a detonation wave. Since the run-to-detonation distance was longer than the 65-mm thickness of the explosive, the orthogonally moving detonation wave interacted with precompressed but unreacted explosive. The radiographic results and computer modeling indicate that the detonation wave was quenched as it propagated into the preshocked X-0219 explosive.

The three desensitizing experiments on PBX-9502 were constituted similar to that of baratol and X-0219. A different desensitizing pressure was used in each of the three experiments by adjusting the speed of the steel flyer plate. One test had a plate speed of 0.5 km/s that resulted in a 2.5 GPa input pressure, the second experiment had a plate speed of 0.88 km/s which produced a 5.5 GPa desensitizing pressure, and the last experiment had a plate speed of 1.8 km/s that induced a pressure of 14.0 GPa. Reproductions of the dynamic radiographs of the experiments are shown in Figs. 43-45. Figure 43 corresponds to a preshock pressure of 2.5 GPa, Fig. 44 corresponds to a preshock of 5.5 GPa, and Fig. 45 corresponds to a pressure of 14.0 GPa. At preshock pressures of 2.5 and 5.5 GPa in PBX-9502, the run-to-detonation distance[8] is much longer than the thickness of explosive and, hence, the detonation wave proceeds into precompressed explosive. From an examination of the radiographs and from numerical calculations similar to those performed for baratol,[8] desensitization of the PBX-9502 by preshocking caused the detonation wave to be quenched. The agreement between calculations which included a desensitization parameter and experiment is shown in Fig. 46. In the third experiment with a preshock pressure of about 14.0 GPa, the run-to-detonation distance is nearly 7.0 mm which is much less than the thickness of the explosive. Hence, at the time of the radiograph in Fig. 45, the observed flow pattern resulted from the interaction of two detonation waves.

The failure of a detonation wave to continue to propagate when the front interacts with an explosive that has been previously shocked has been studied experimentally by radiographic techniques using PHERMEX and has been modeled numerically with good success. Figure 47 summarizes the results from the desensitizing experiments on insensitive explosives.

ACKNOWLEDGMENTS

The author acknowledges the help of T. R. Neal in preparing the section of this paper dealing with radiographic studies of inert materials. I acknowledge the support of Wm. R. Field so that I could participate in this Cineradiography Conference. Finally, I thank Leah A. Baker for typing this paper.

REFERENCES

1. "LASL PHERMEX Data Volumes I, II, and III," University of California Press, Berkeley and Los Angeles, California, 1980, C. L. Mader, Ed.

2. T. Neal, "Perpendicular Explosive Drive and Oblique Shocks," Proceedings Sixth Symposium (International) on Detonation, U. S. Naval Ordnance, White Oak, August 1976.

3. T. Neal, "Mach Waves and Reflected Rarefactions in Aluminum," JAP 46, 2521 (1975).

4. T. Neal, "Dynamic Determinations of the Grüneisen Coefficient in Aluminum and Aluminum Alloys for Densities up to 6 Mg/m^3," Phys. Rev. B 14, 5172 (1976).

5. T. Neal, "Second Hugoniot Relationship for Solids," J. Phys. Chem. Solids 38, 225 (1977).

6. B. R. Breed and Douglas Venable, "Dynamic Observations of the Course of a Shock-Induced Phase Transition in Antimony," JAP 39, 3222 (1968).

7. Richard D. Dick, "Insensitive Explosive Studies Using PHERMEX," Proceedings of the Flash Radiography Symposium of the American Society for Nondestructive Testing, Houston, Texas, September 1976, Lawrence E. Bryant, Jr., Ed.

8. C. L. Mader and R. Dick, "Explosive Desensitization by Preshocking," Internationale Jahrestagung 1979 - Combustion and Detonation Processes, Karlsruhe, Bundesrepublik, Deutschland, June 1979.

9. Charles L. Mader, "Numerical Model of Detonations," University of California Press, Berkeley (1979).

10. "LASL Shock Hugoniot Data," University of California Press, Berkeley, 1980, Stanley P. Marsh, Ed.

11. H. M. Sternberg and D. Piacesi, "Interaction of Oblique Detonation Waves with Iron," Physics of Fluids 4, 1307 (1966).

12. Russell L. Duff and F. Stanley Minshall, "Investigation of a Shock-Induced Transition in Bismuth," Phy. Rev. 108, 1207 (1957).

13. Donald B. Larson, "A Shock-Induced Phase Transition in Bismuth," JAP 38, 1541 (1967).

14. R. H. Warnes, "Investigation of a Shock-Induced Phase Transition in Antimony," JAP 38, 4629 (1967).

15. R. D. Dick, "Shock-Wave Compression of Benzene, Carbon Disulfide, Carbon Tetrachloride, and Liquid Nitrogen," J. Chem. Phys. 52, 6021 (1970).

16. Stephen A. Sheffield, "Shock-Induced Reaction in Carbon Disulfide," Washington State University, Pullman, Washington, Report - WSU SDI 78-03, June 1978.

FIGURE CAPTIONS

Fig. 1. Schematic of perpendicular drive and the relevant equations.
Fig. 2. Reproduction of a static radiograph of a perpendicular-drive experiment on aluminum.
Fig. 3. Reproduction of the dynamic radiograph of a perpendicular-drive experiment on aluminum.
Fig. 4. Line drawing of the principal features of the radiograph shown in Fig. 3.
Fig. 5. U_s-U_p data on aluminum using the perpendicular-drive technique and radiography.
Fig. 6. Table of values measured from the aluminum experiments.
Fig. 7. Schematic of the oblique-reflection technique for off-Hugoniot measurements.
Fig. 8. Reproduction of the static radiograph of the sound-speed experiment on aluminum.
Fig. 9. Radiograph of the oblique-reflection experiment on aluminum.
Fig. 10. Line drawing of the radiograph in Fig. 9.
Fig. 11. Reproduction of the dynamic radiograph of the regular-reflection experiment on lead.
Fig. 12. Reproduction of the static radiograph of a double-shock experiment on bismuth.
Fig. 13. Reproduction of the dynamic radiograph showing a two-shock character in bismuth.
Fig. 14. Line drawing of the essential features of the bismuth experiment.
Fig. 15. Reproduction of the dynamic radiograph showing the two-shock structure in antimony.
Fig. 16. Line drawing of the main features of the antimony experiment.
Fig. 17. Reproduction of the dynamic radiograph for the two-shock experiment on carbon disulfide.
Fig. 18. A description of several explosives.
Fig. 19. Schematic diagram of the corner-turning experiments.
Fig. 20. Typical radiographic geometry for the corner-turning experiments.
Fig. 21. Reproduction of a typical static radiograph of the corner-turning experiments.
Fig. 22. Reproduction of a dynamic radiograph of a corner-turning experiment on X-0219.
Fig. 23. Reproduction of a dynamic radiograph of a corner-turning experiment on X-0219 at a later time than Fig. 22.
Fig. 24. Reproduction of a dynamic radiograph of a corner-turning experiment on X-0219 at a later time than Fig. 23.
Fig. 25. Reproduction of a dynamic radiograph of a corner-turning experiment on X-0291.
Fig. 26. Reproduction of a dynamic radiograph of a corner-turning experiment on X-0291 at a later time than Fig. 25.
Fig. 27. Reproduction of a dynamic radiograph of a corner-turning experiment on X-0291 at a later time than Fig. 26.
Fig. 28. Reproduction of a dynamic radiograph of a corner-turning experiment on PBX-9502.
Fig. 29. Reproduction of a dynamic radiograph of a corner-turning experiment on PBX-9502 at a time later than Fig. 28.
Fig. 30. Reproduction of a dynamic radiograph of a corner-turning experiment on PBX-9502 at a time later than Fig. 29.
Fig. 31. Reproduction of a dynamic radiograph of a corner-turning experiment on PBX-9501.
Fig. 32. Reproduction of a dynamic radiograph of a corner-turning experiment on PBX-9501 at a time later than Fig. 31.
Fig. 33. Reproduction of a dynamic radiograph of a corner-turning experiment on PBX-9501 at a time later than Fig. 32.
Fig. 34. A composite of the three tests on X-0219.

Perpendicuiar drive

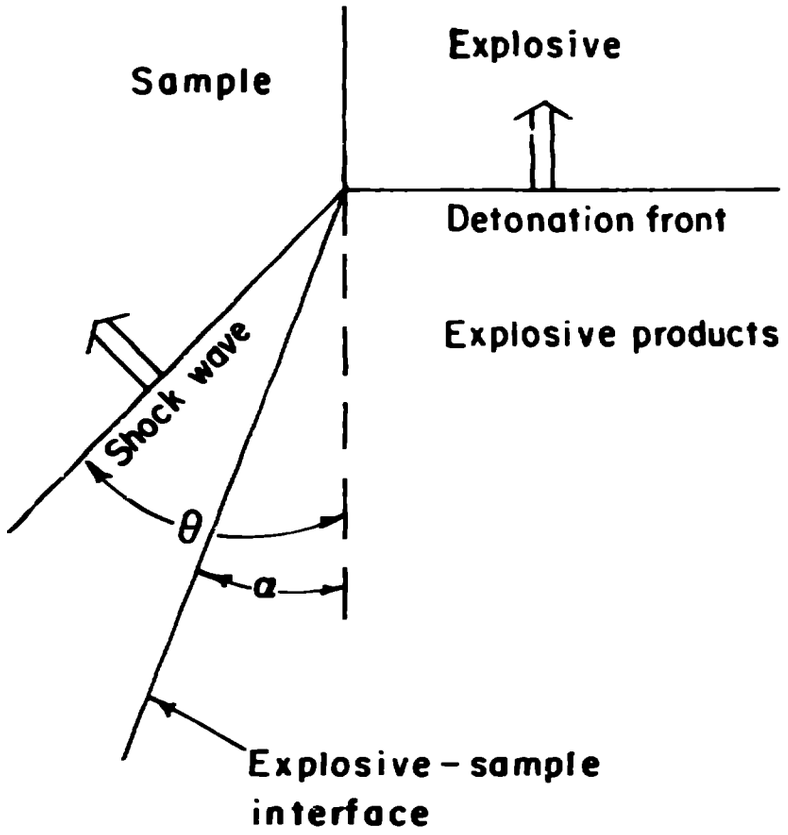

$$U_s = D \sin \theta$$

$$U_p = \frac{D \tan \alpha}{\cos \theta + \sin \theta \tan \alpha}$$

U_s = shock velocity

U_p = particle velocity

D = detonation velocity

Fig. 1

Fig. 2

Fig. 3

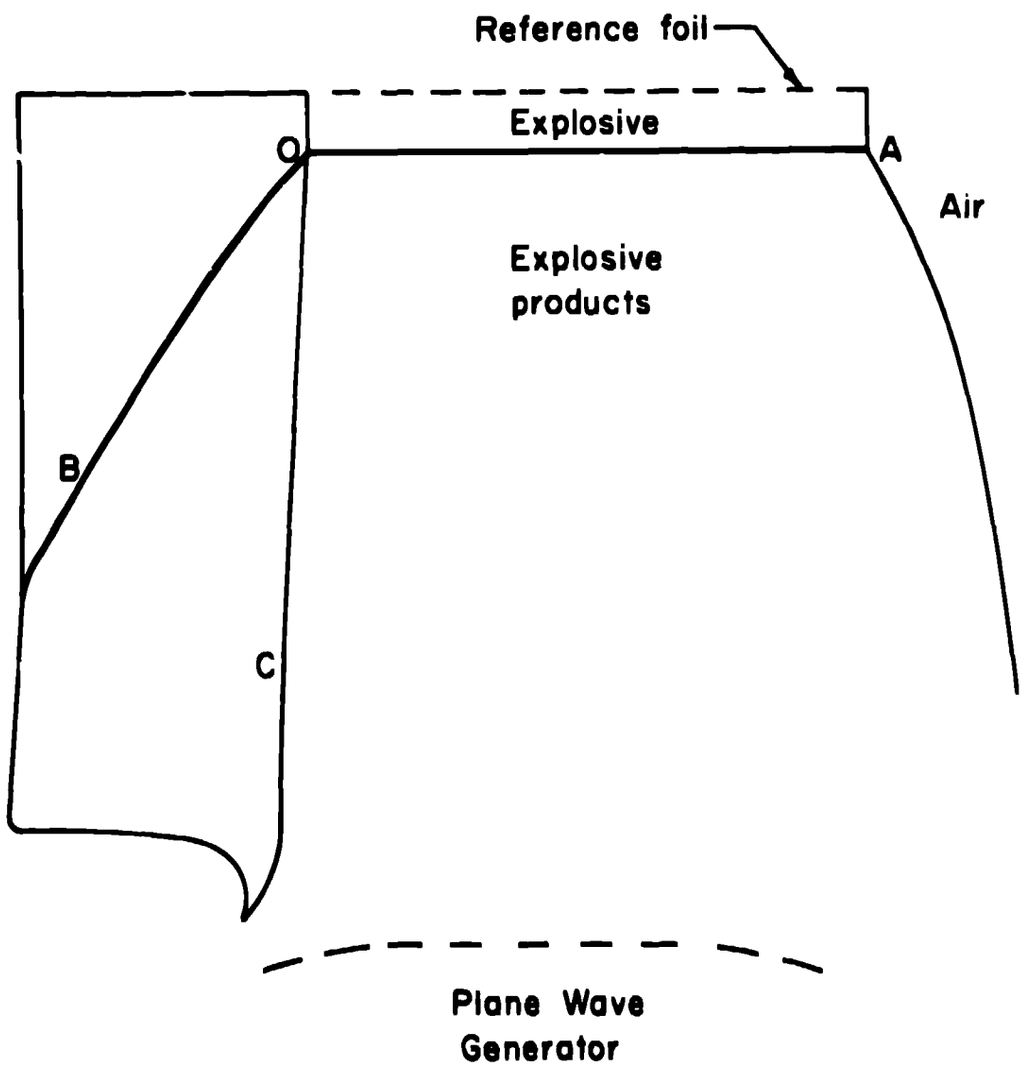
Reference foil
Explosive
O
A
Air
Explosive
products
B
C
Plane Wave
Generator

Fig. 4

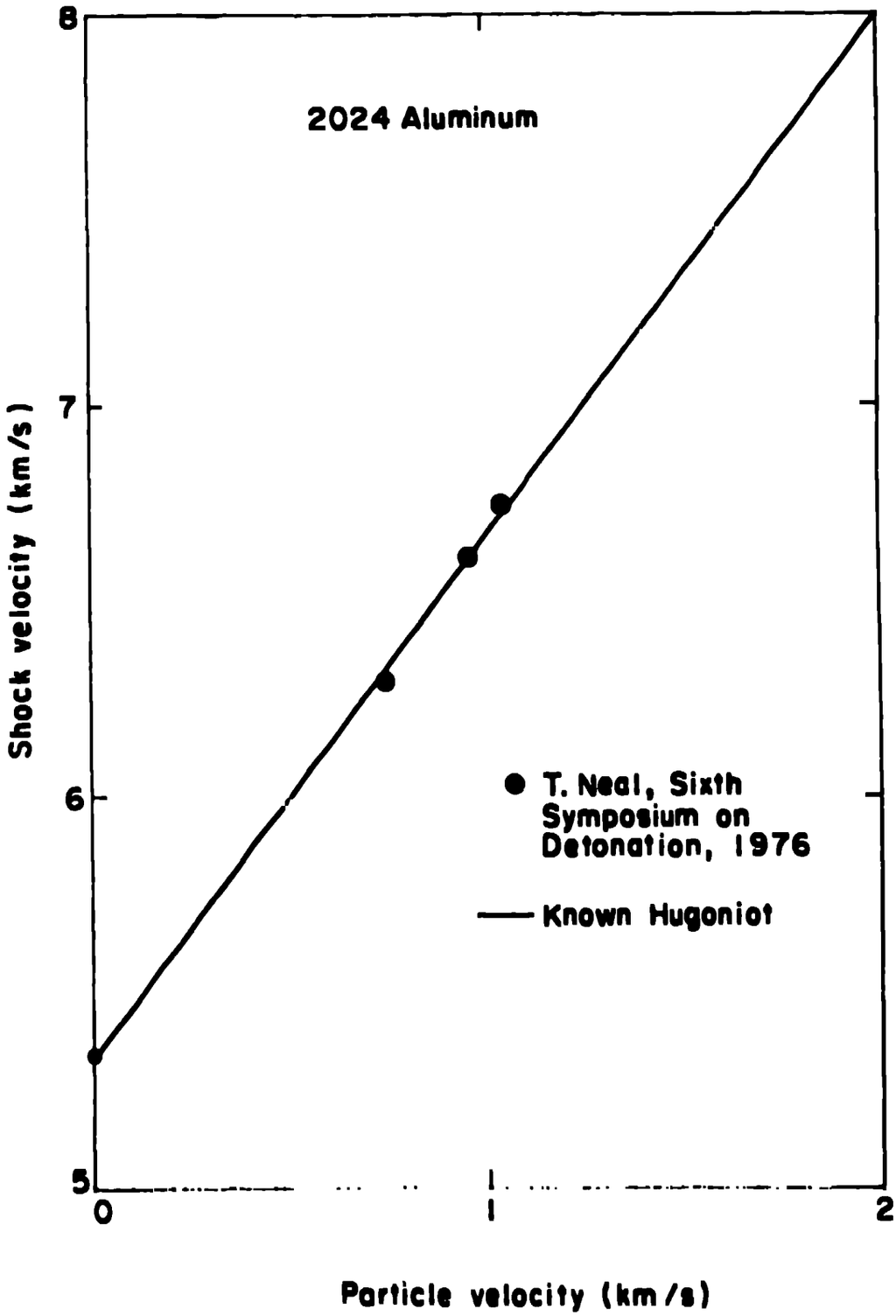
2024 Aluminum
Shock velocity (km/s)
Particle velocity (km/s)
8
7
6
5
0
1
2
T. Neal, Sixth Symposium on Detonation, 1976
Known Hugoniot

Fig. 5

Aluminum Hugoniot data using perpendicular drive and radiography

HE	θ^a (°)	U_s (km/s)	P (GPa)	α (°)	α^a (°)	U_p (km/s)	P (GPa)
TNT	65.49	6.278	12.5	2.71	2.87	0.751	13.1
Comp B	56.72	6.617	17.8	4.27	4.22	0.957	17.7
9404	49.97	6.738	19.9	4.87	4.82	1.048	19.7

[a] Measured directly

Fig. 6

Oblique reflection

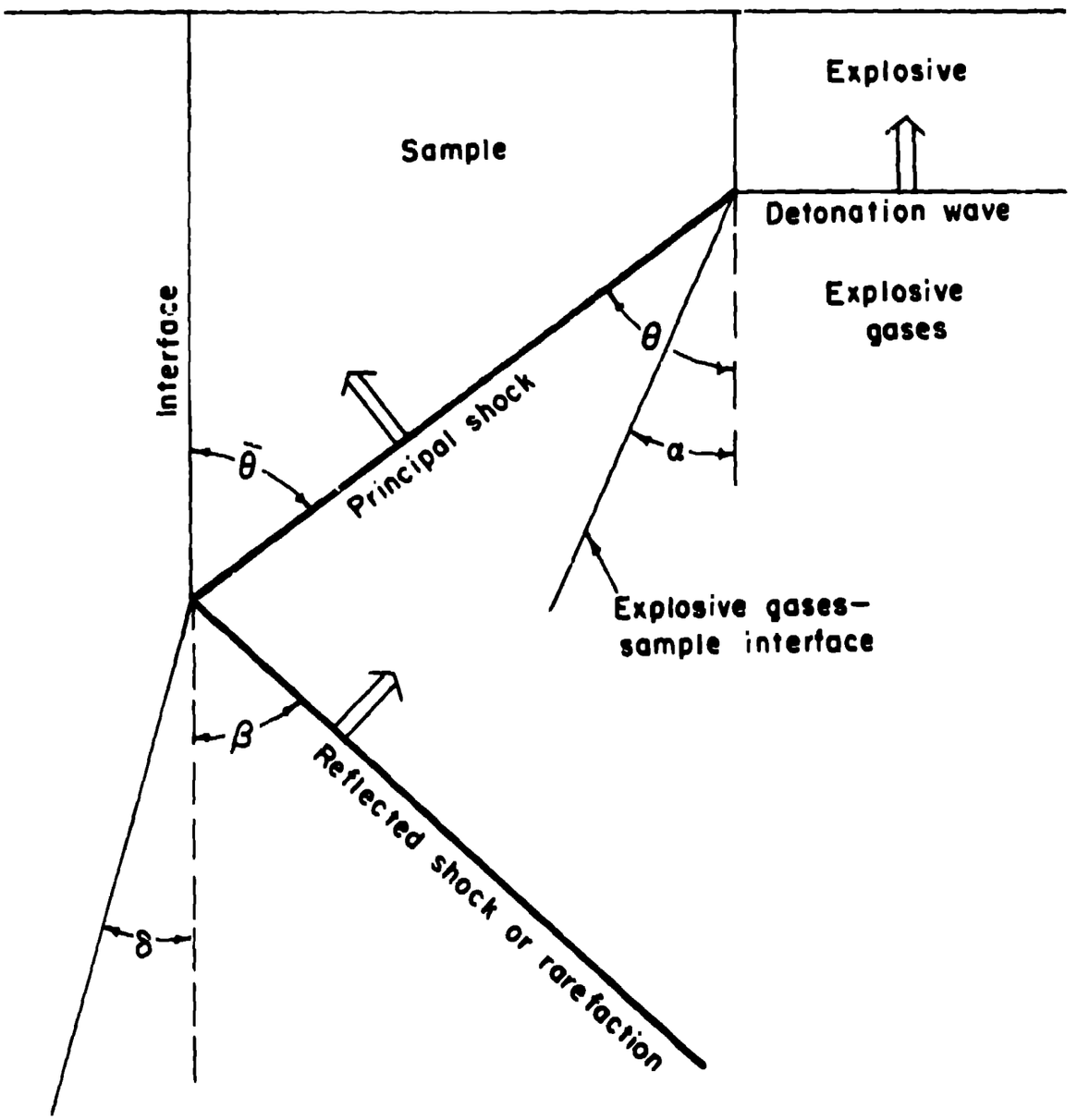

Fig. 7

Fig. 8

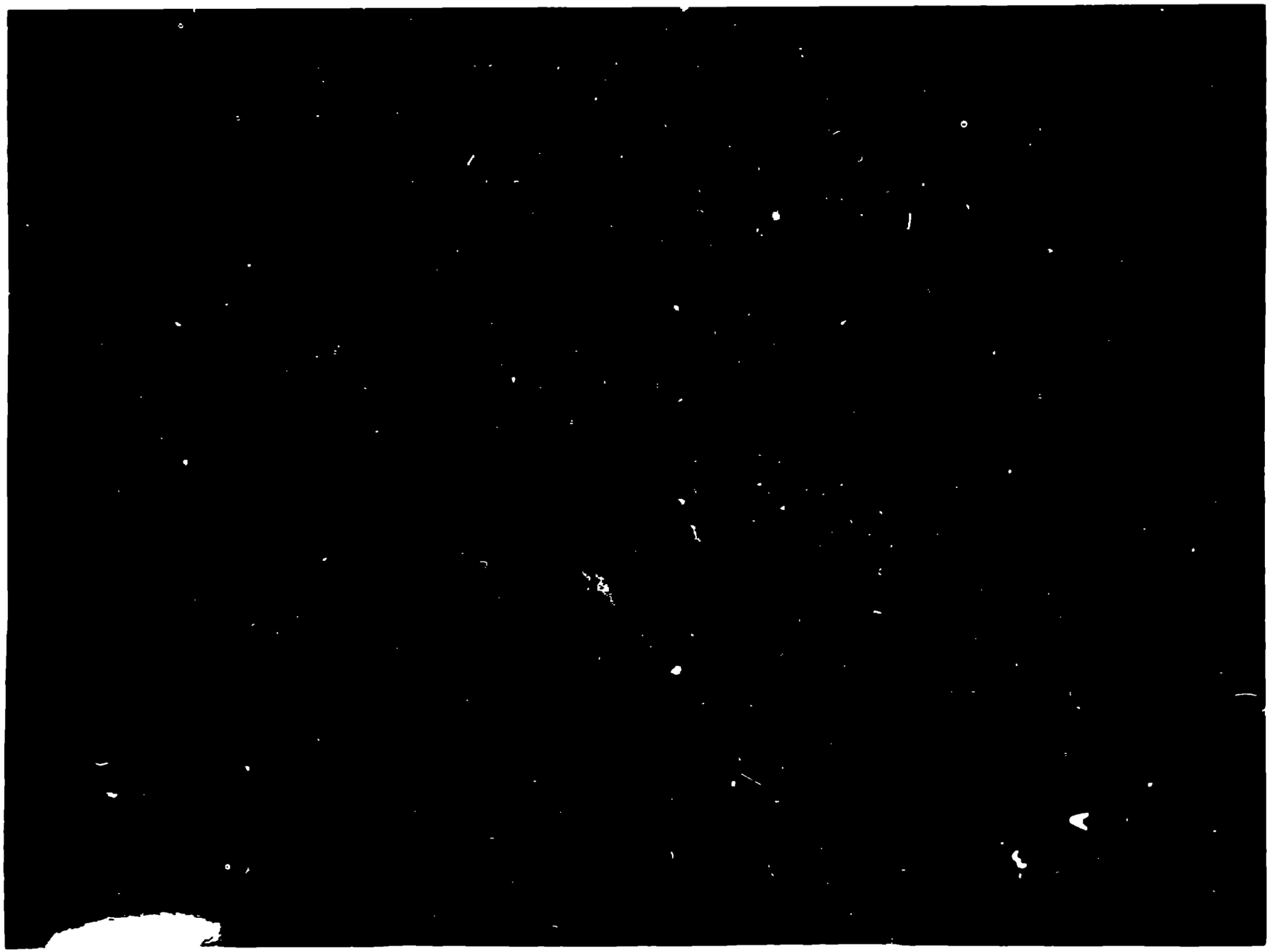

Fig. 9

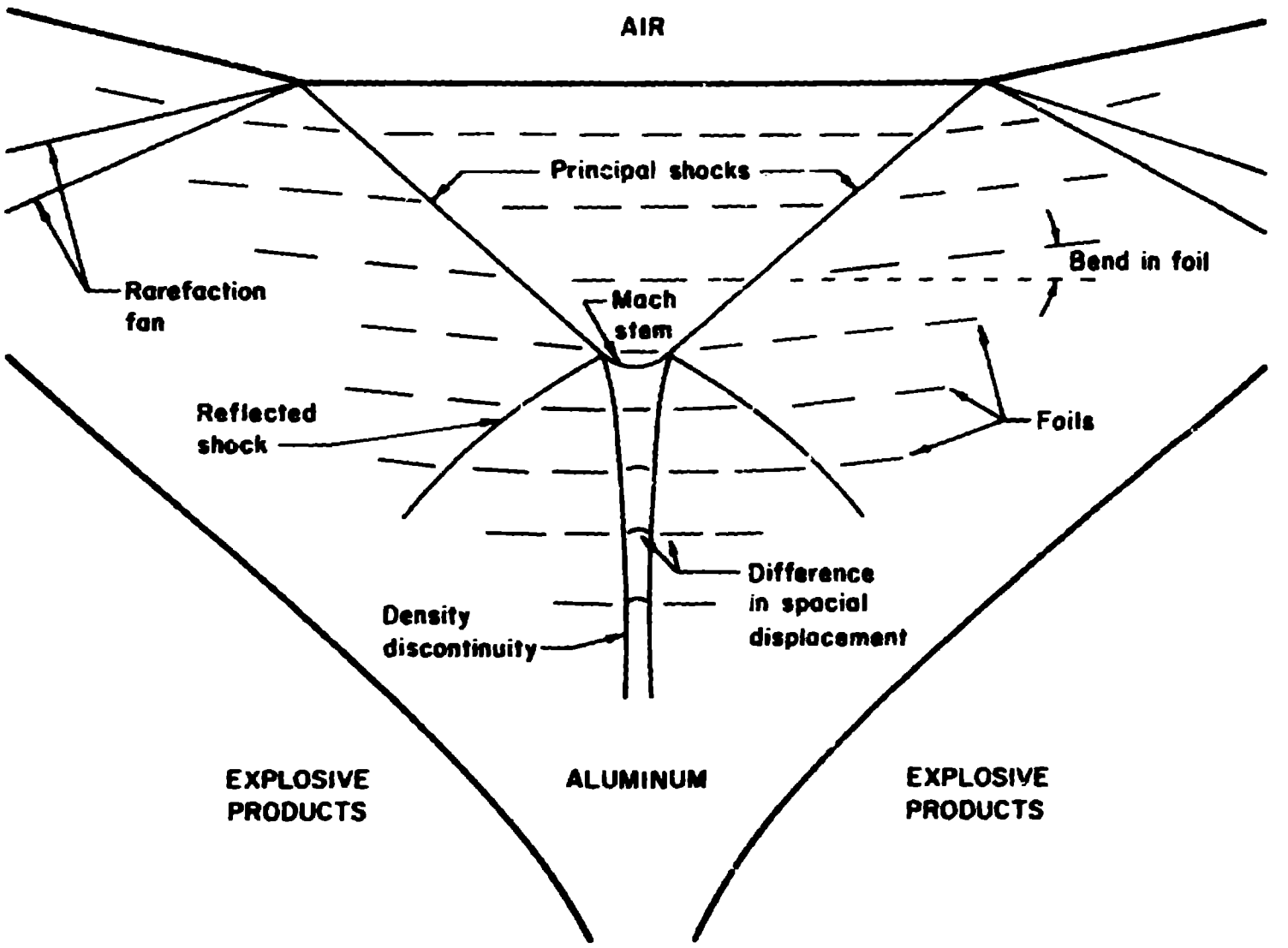
AIR
Principal shocks
Bend in foil
Rarefaction fan
Mach stem
Reflected shock
Foils
Difference in spacial displacement
Density discontinuity
EXPLOSIVE PRODUCTS
ALUMINUM
EXPLOSIVE PRODUCTS

Fig. 10

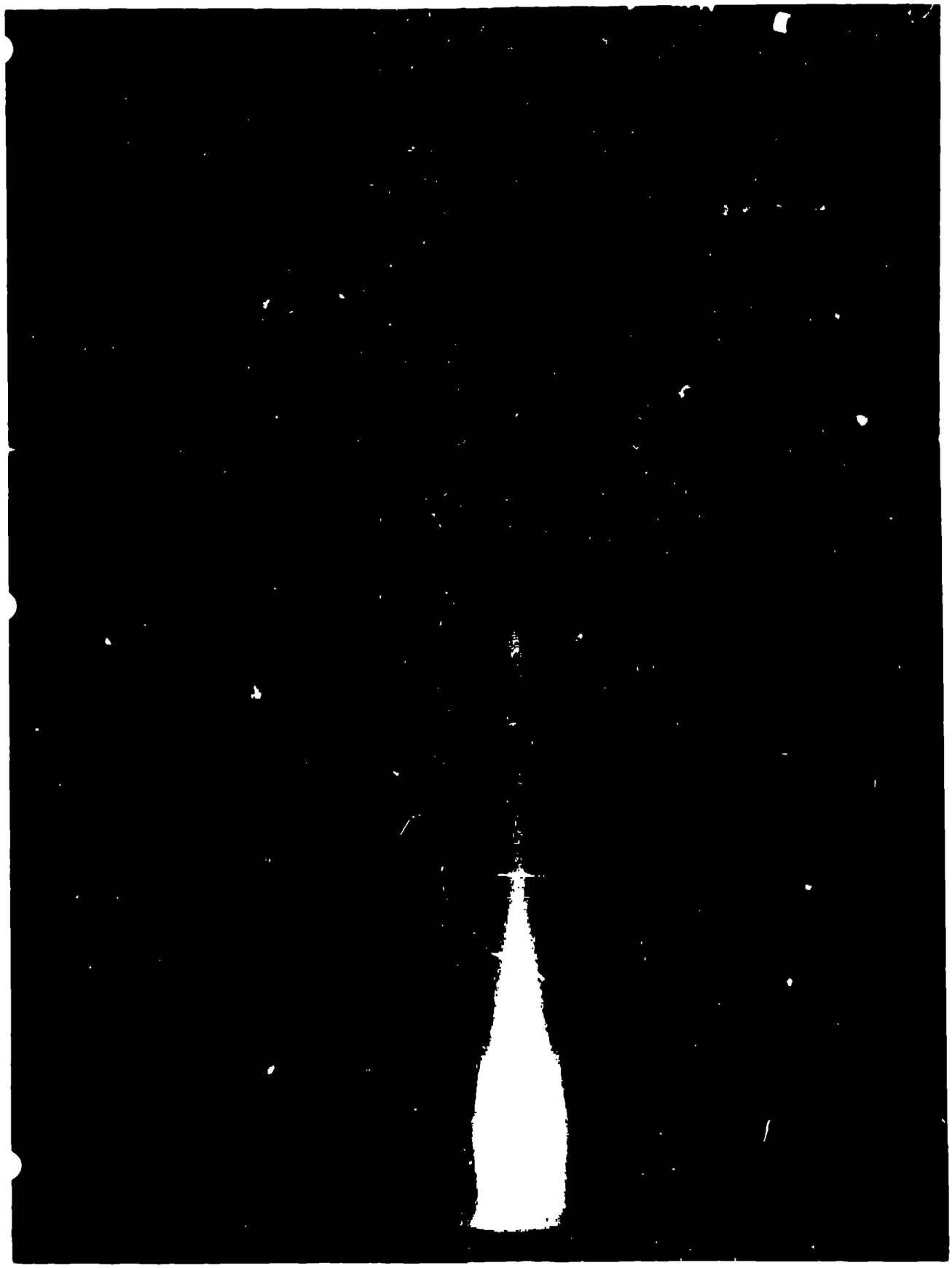

Fig. 11

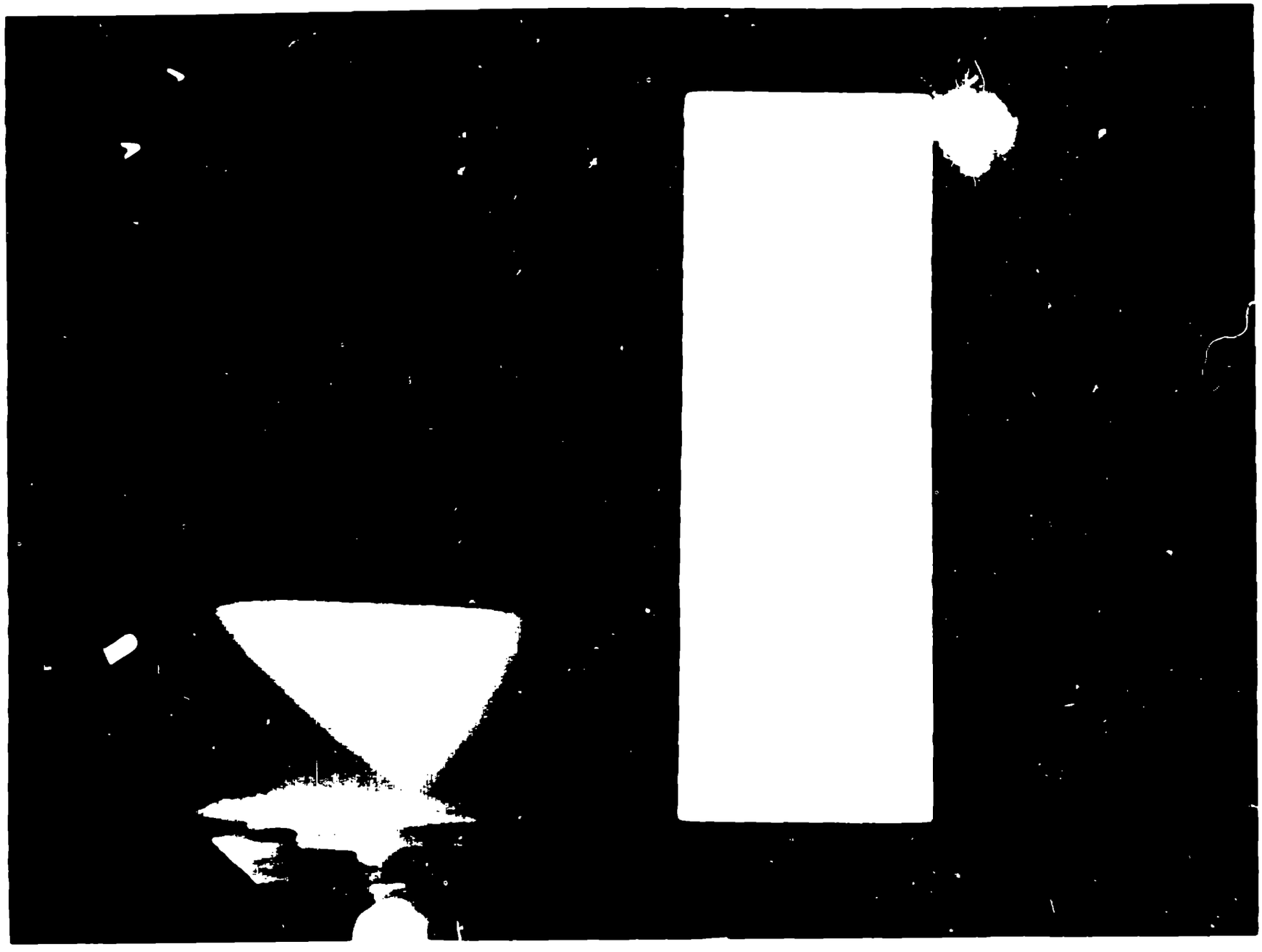

Fig. 12

Fig. 13

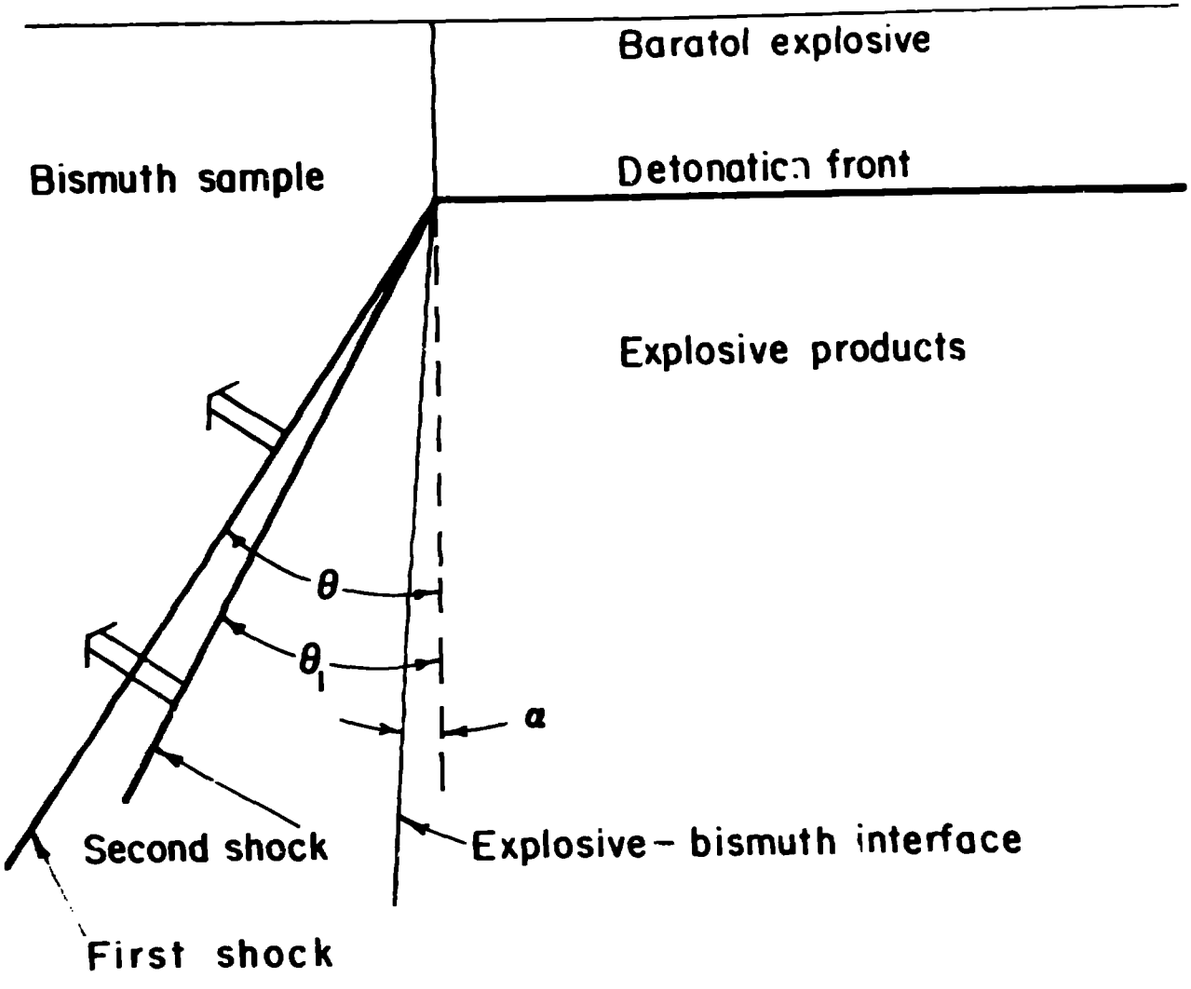
Baratol explosive
Bismuth sample
Detonation front
Explosive products
θ
θ1
α
Second shock
Explosive – bismuth interface
First shock

Fig. 14

Fig. 15

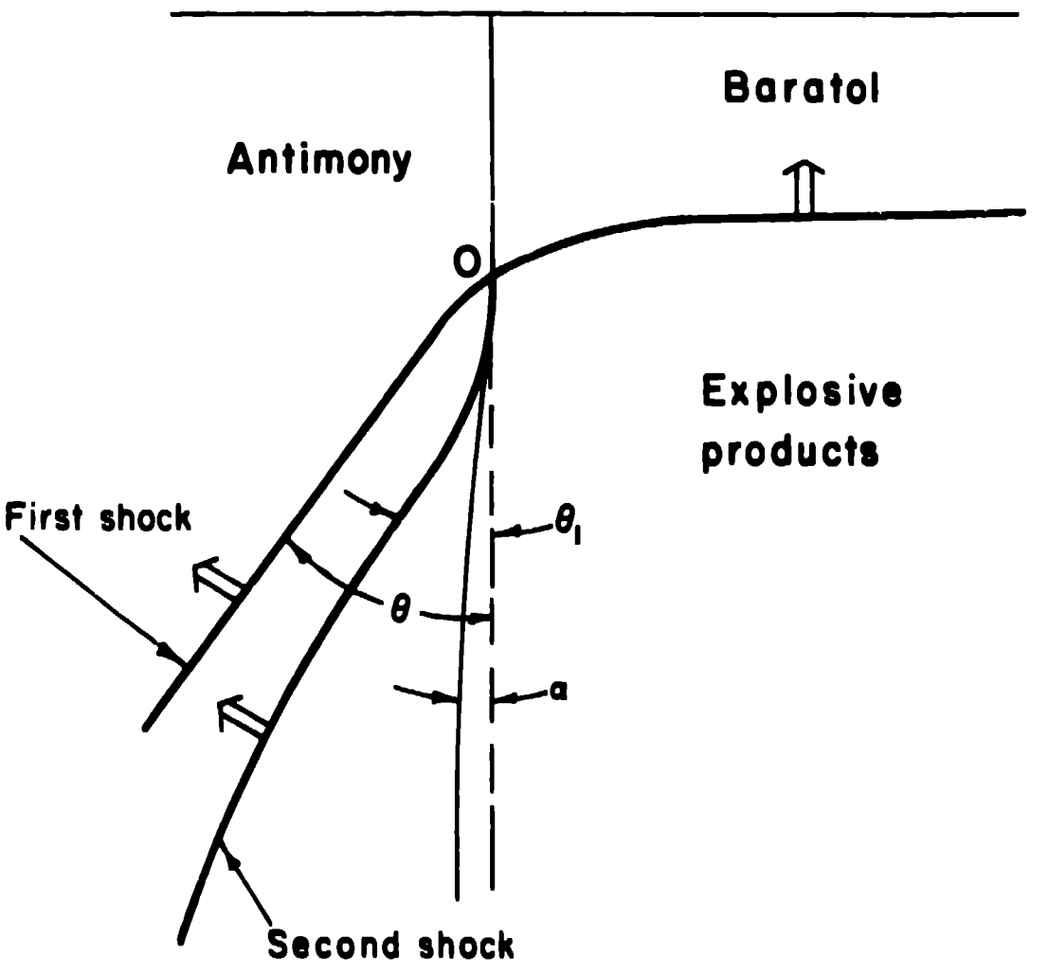
Baratol
Antimony
O
Explosive
products
First shock
θ_1
θ
a
Second shock

Fig. 16

Fig. 17

EXPLOSIVES DESCRIPTION

PBX-9501	95 HMX / 2.5 Estane / 2.5 BDNPA and BDNPF
PBX-9502 (X-0290)	95 TATB/5 Kel-F 800
X-0219	90 TATB/10 Kel-F 800
X-0291	92.5 TATB / 7.5 Kel-F 800
Baratol	76 Barium nitrate / 24 TNT

Fig. 18

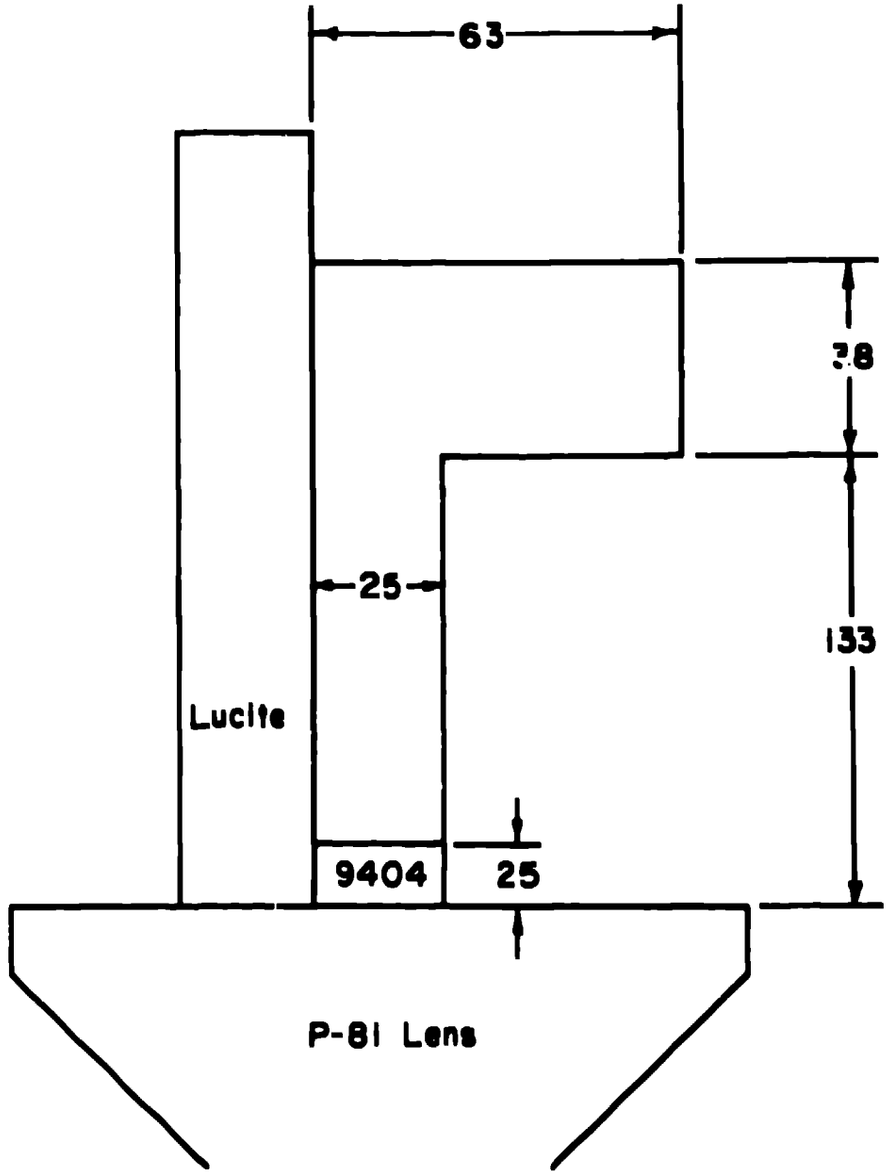

Fig. 19

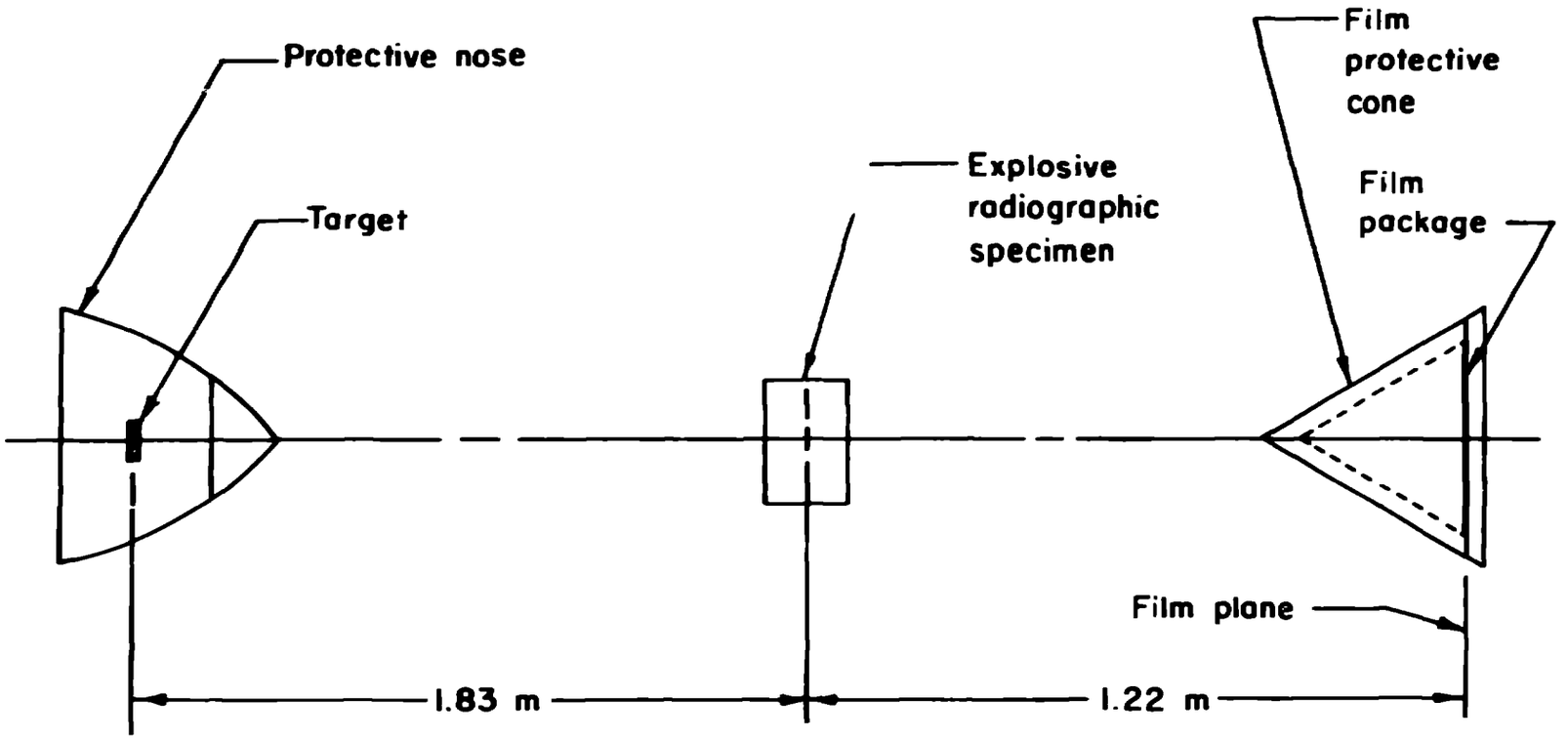
Protective nose
Target
Explosive
radiographic
specimen
Film
protective
cone
Film
package
Film plane
1.83 m
1.22 m

Fig. 20

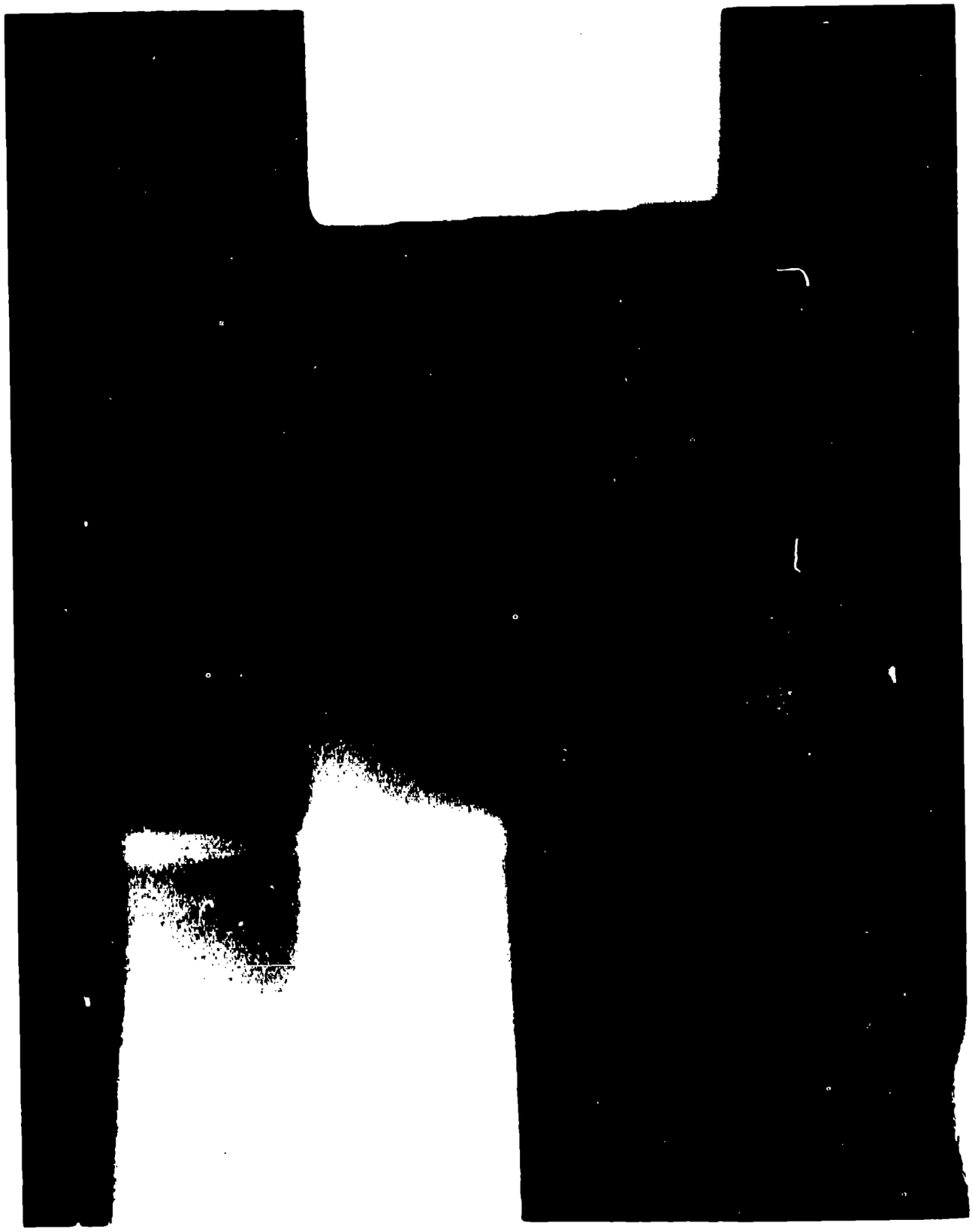

Fig. 21

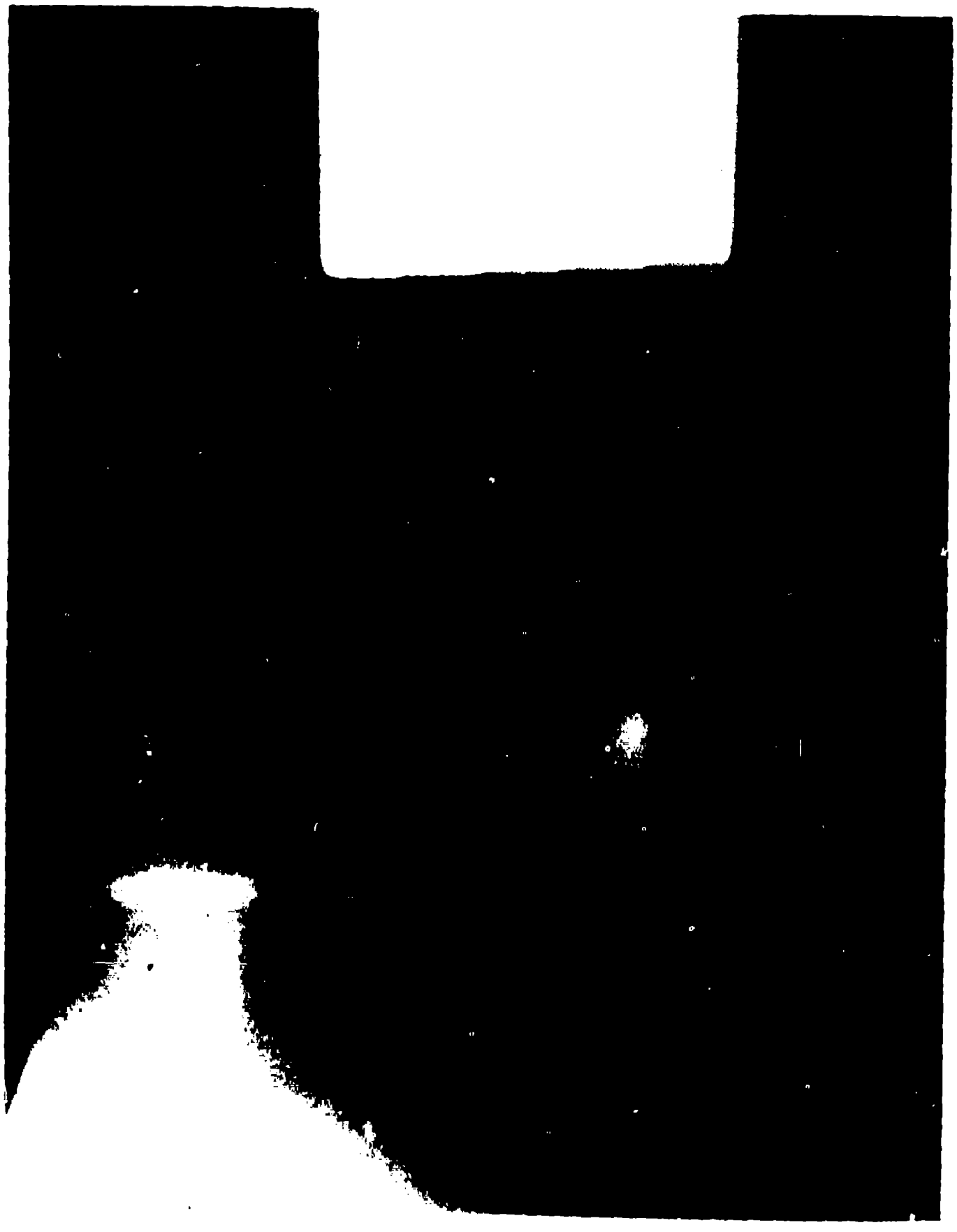

Fig. 22

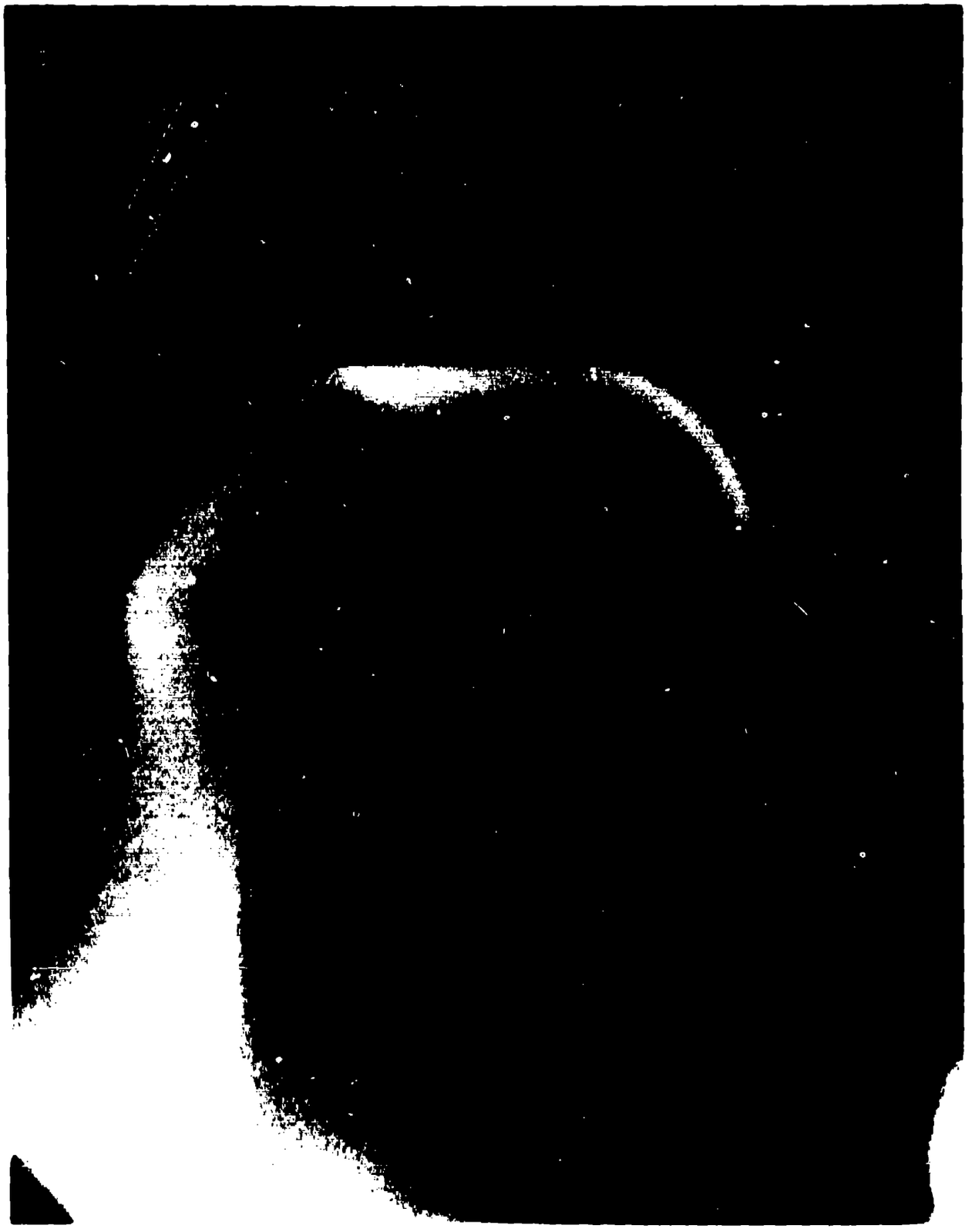

Fig. 23

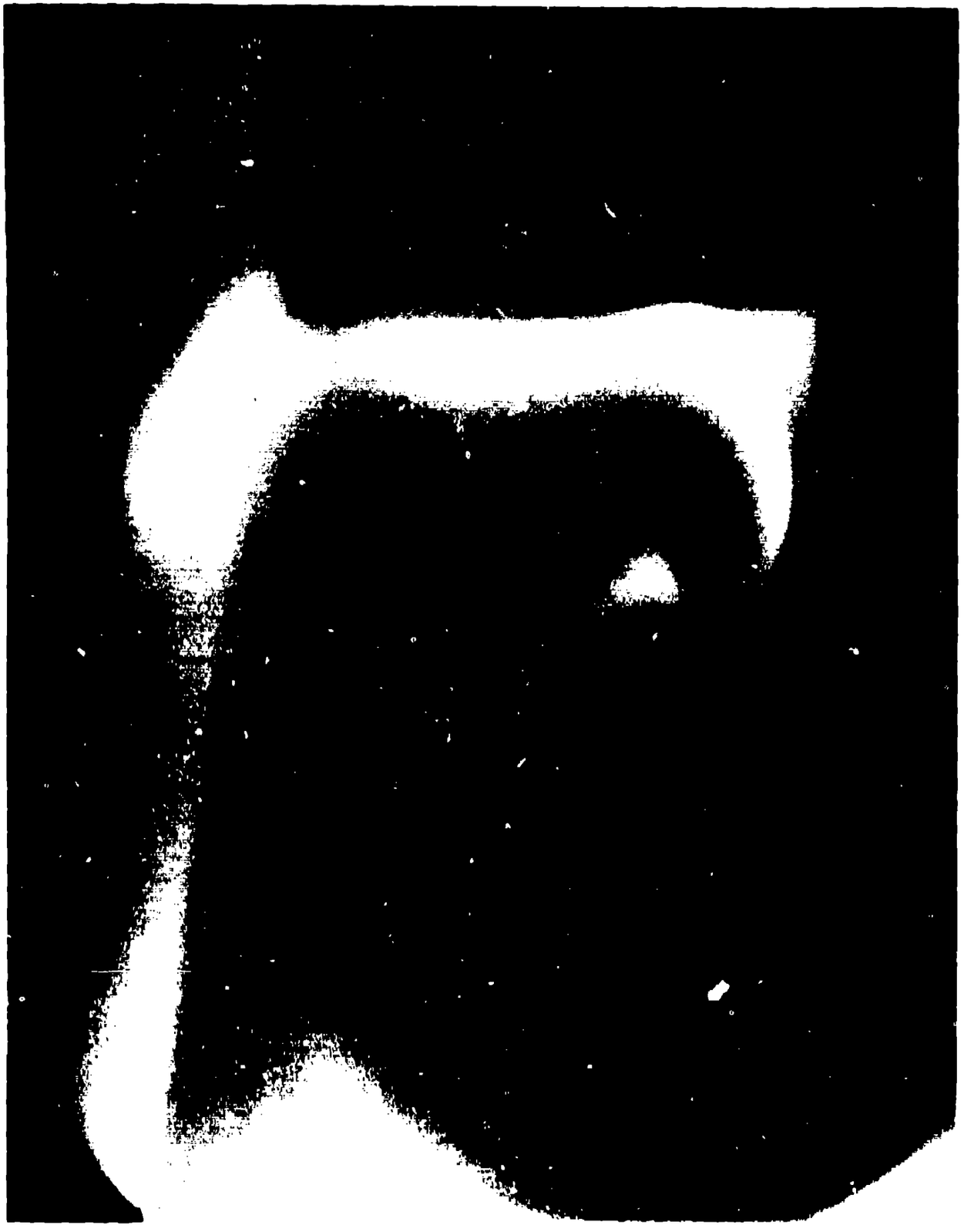

Fig. 24

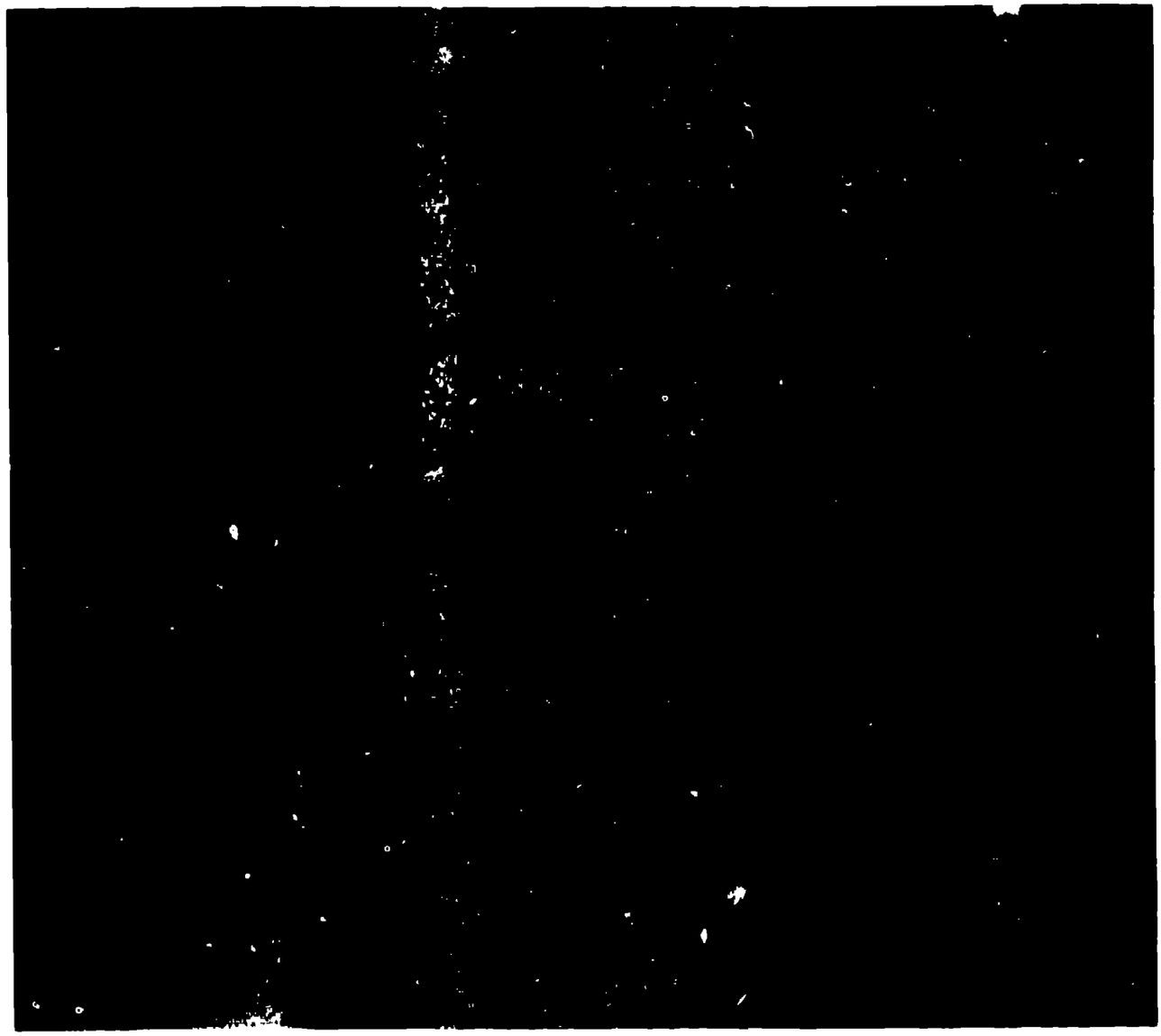

Fig. 25

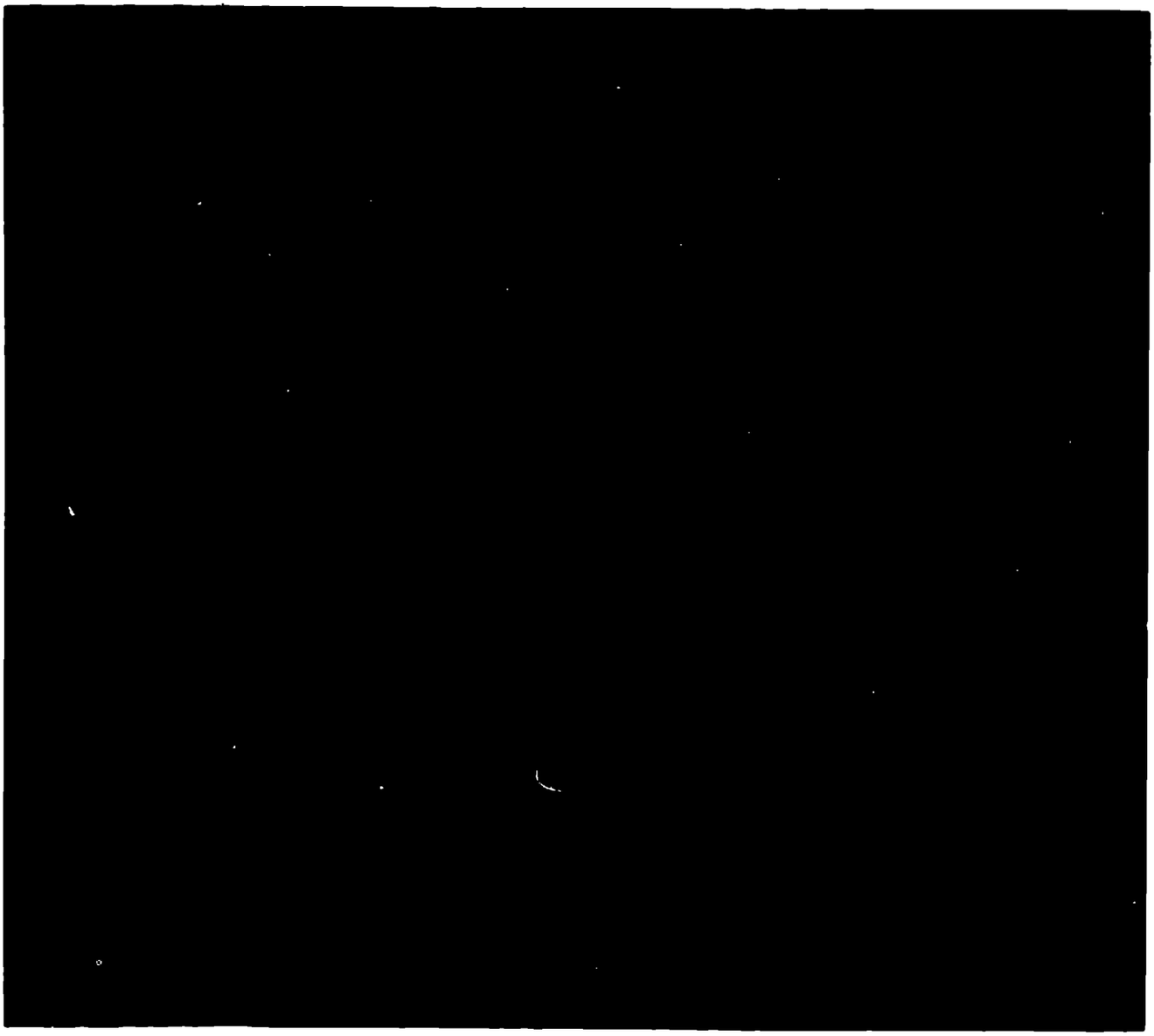

Fig. 26

Fig. 27

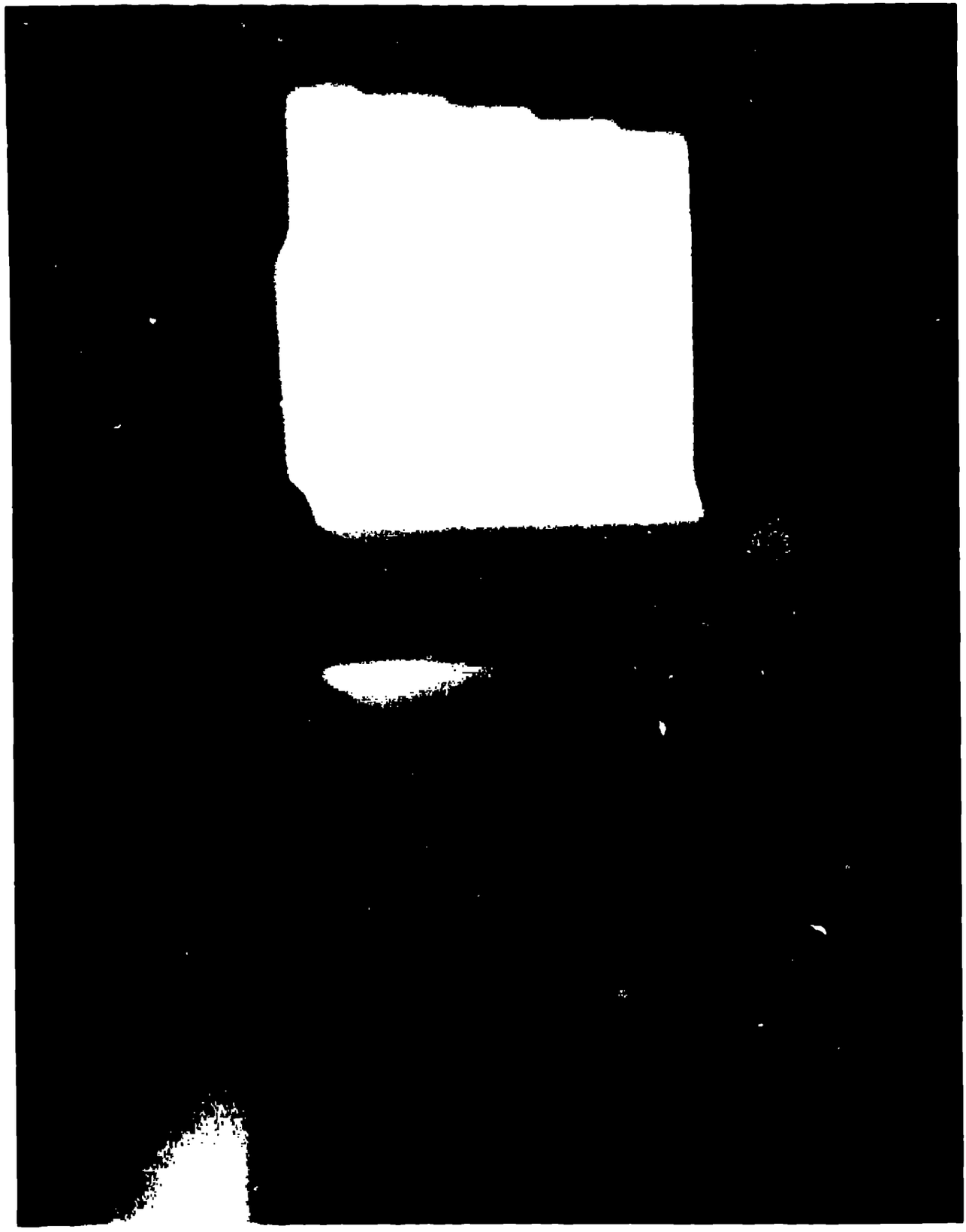

Fig. 28

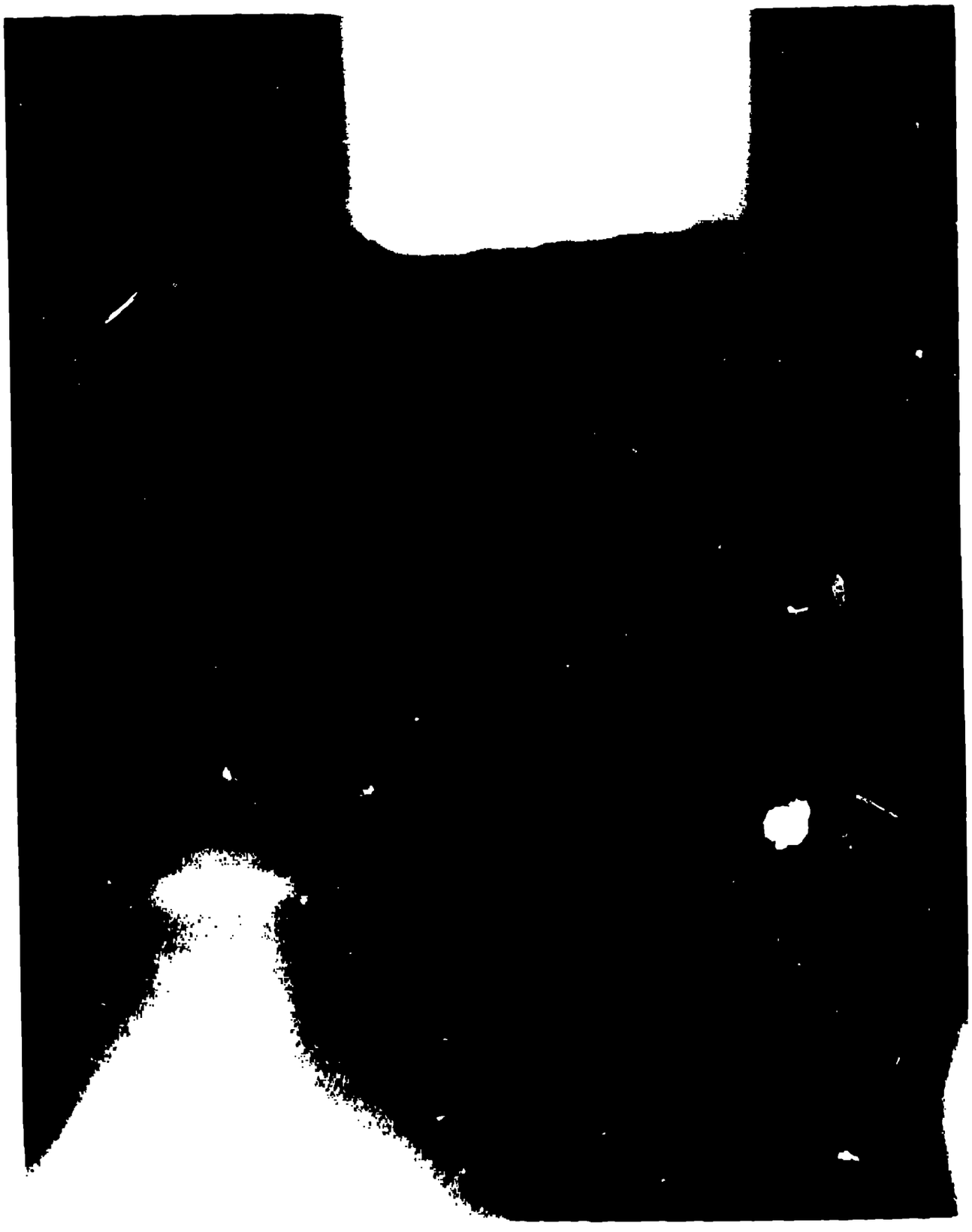

Fig. 29

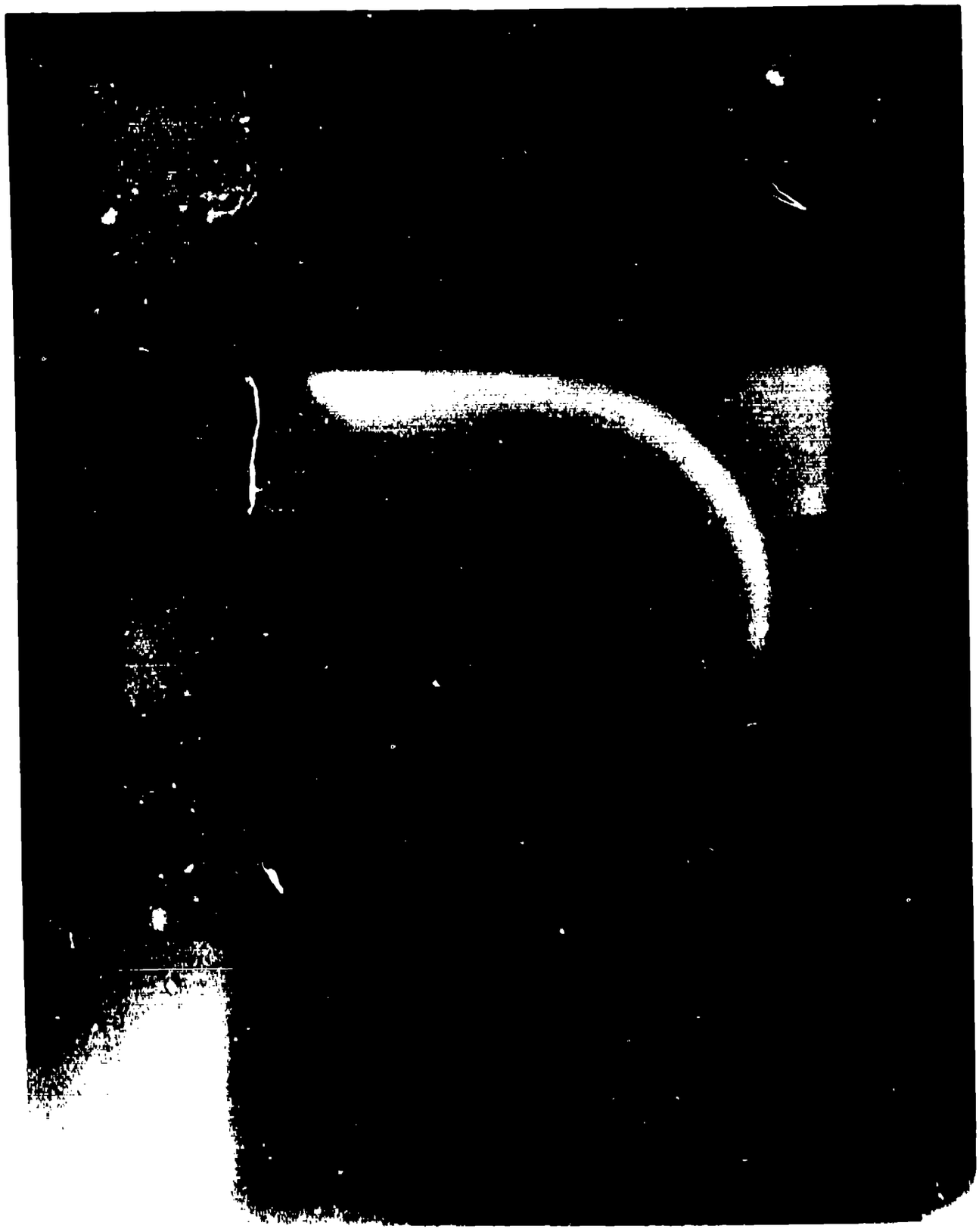

Fig. 30

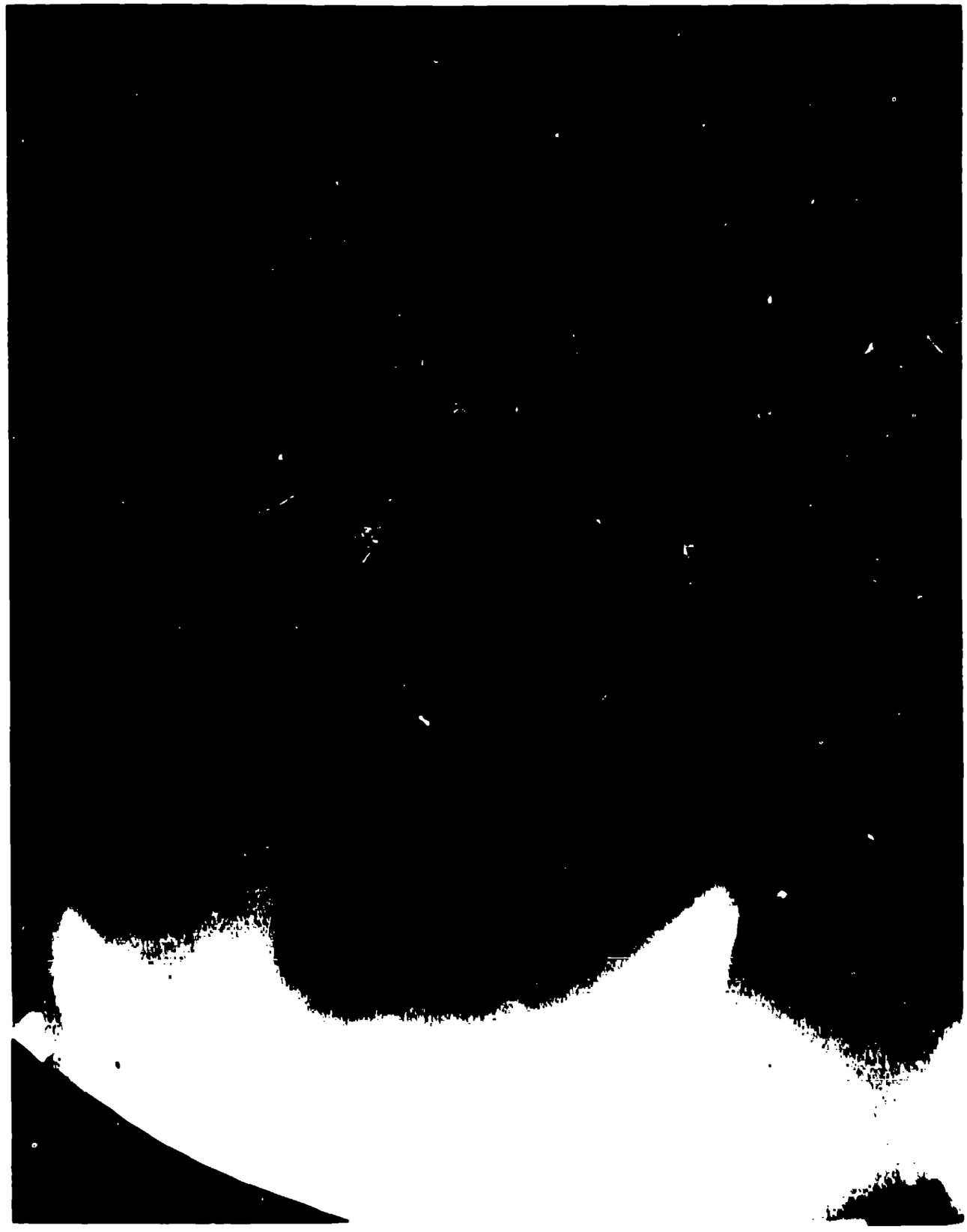

Fig. 31

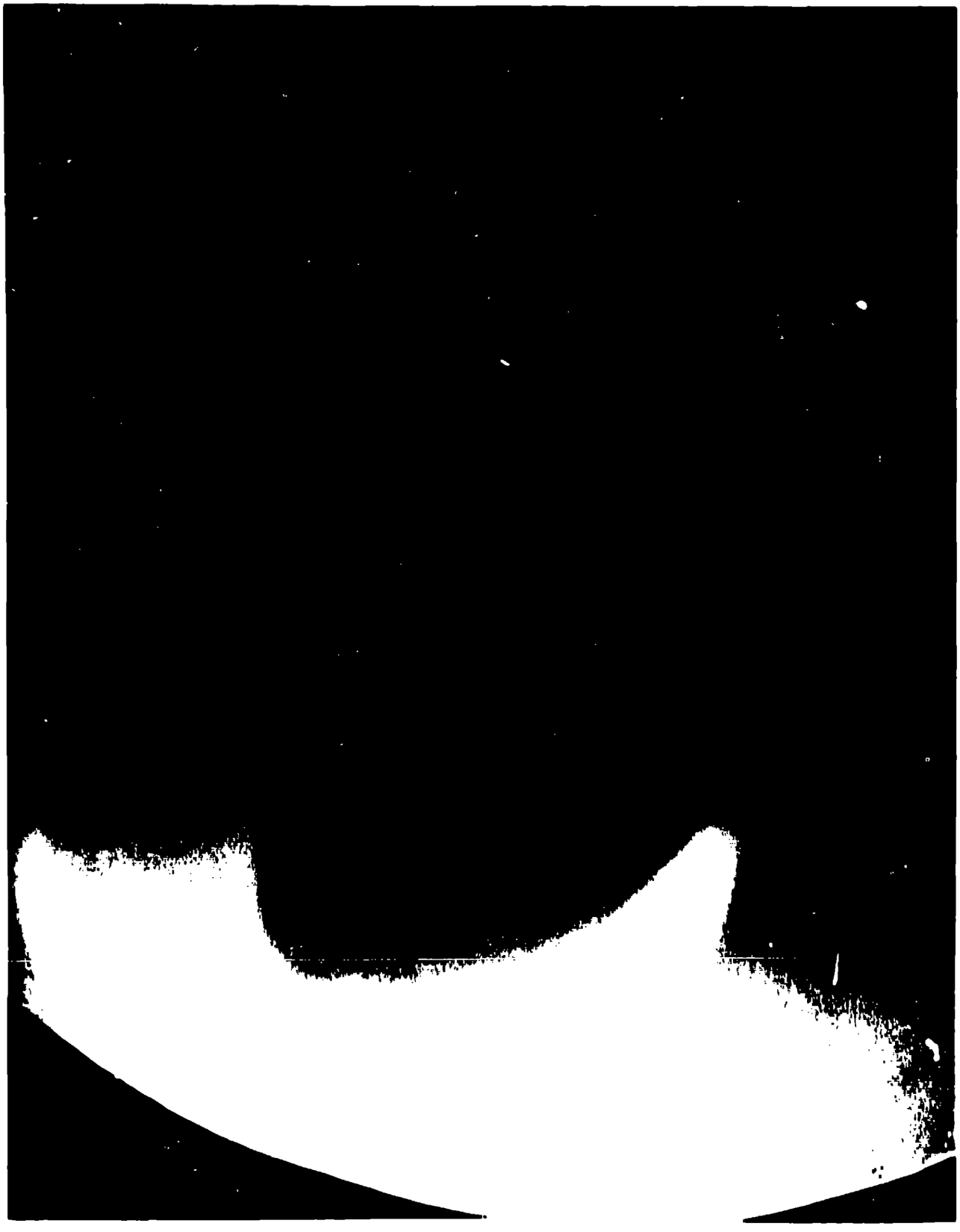

Fig. 32

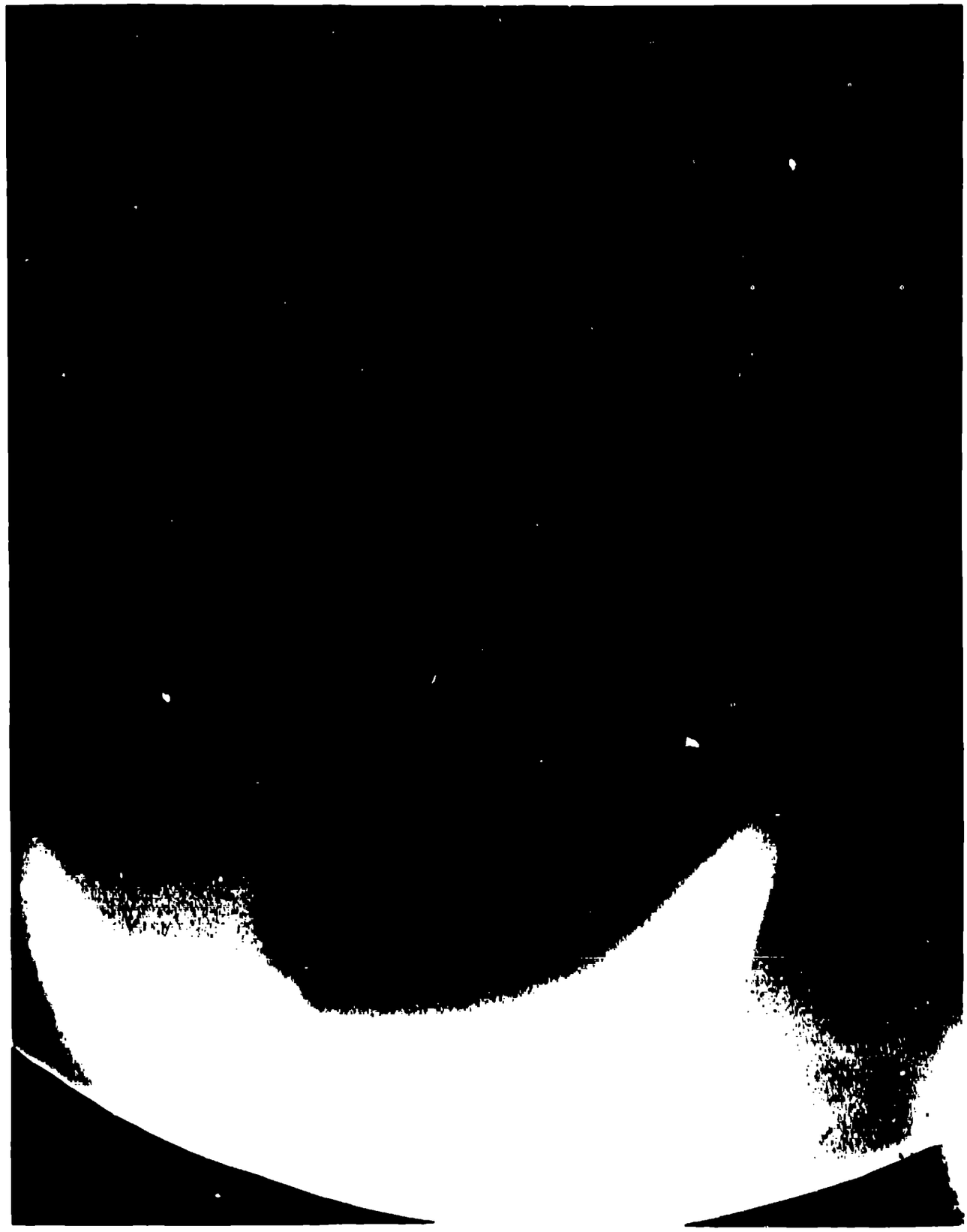

Fig. 33

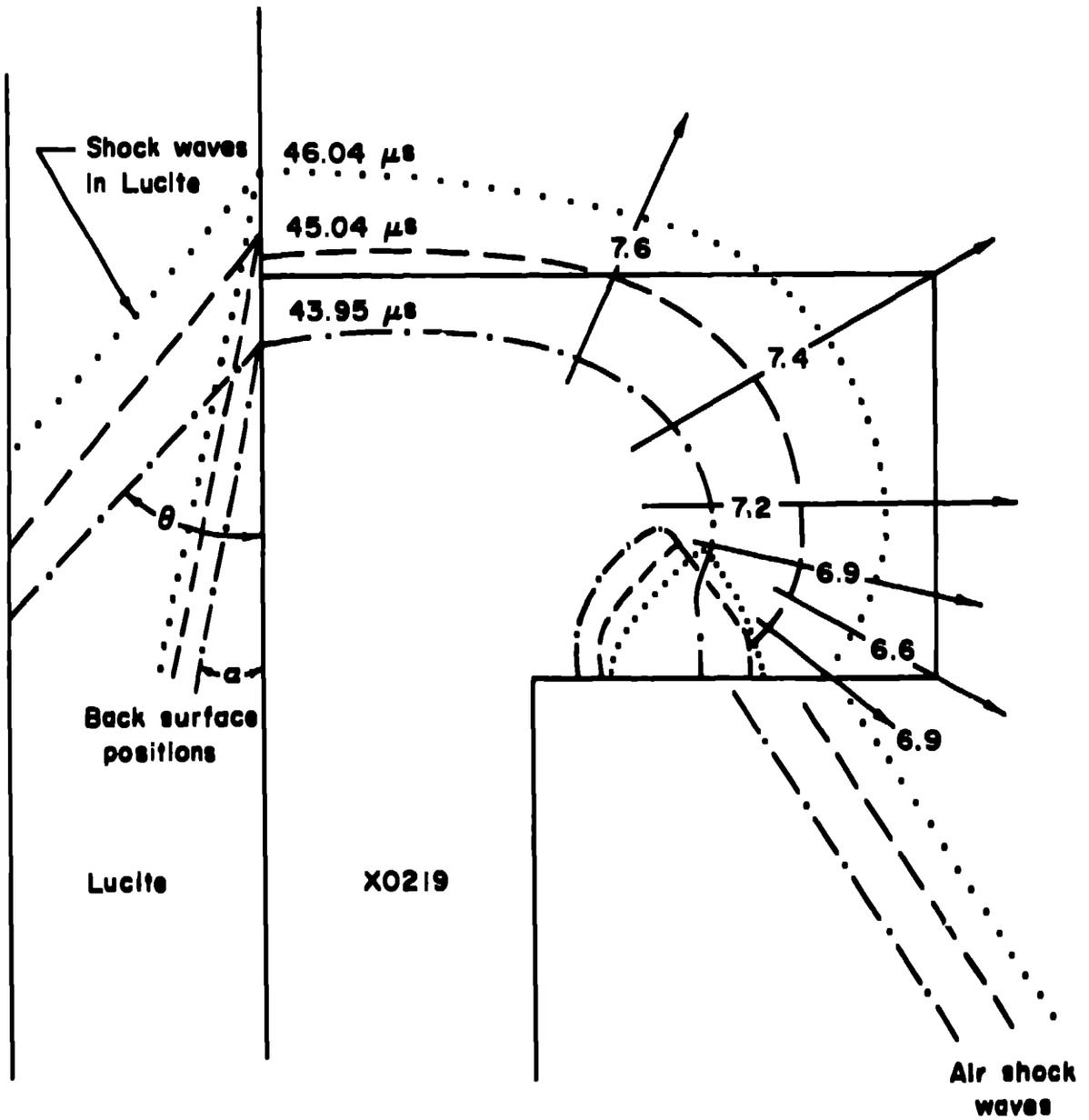
Shock waves
In Lucite
46.04 μs
45.04 μs
43.95 μs
7.6
7.4
7.2
6.9
6.6
6.9
θ
α
Back surface
positions
Lucite
X0219
Air shock
waves

Fig. 34

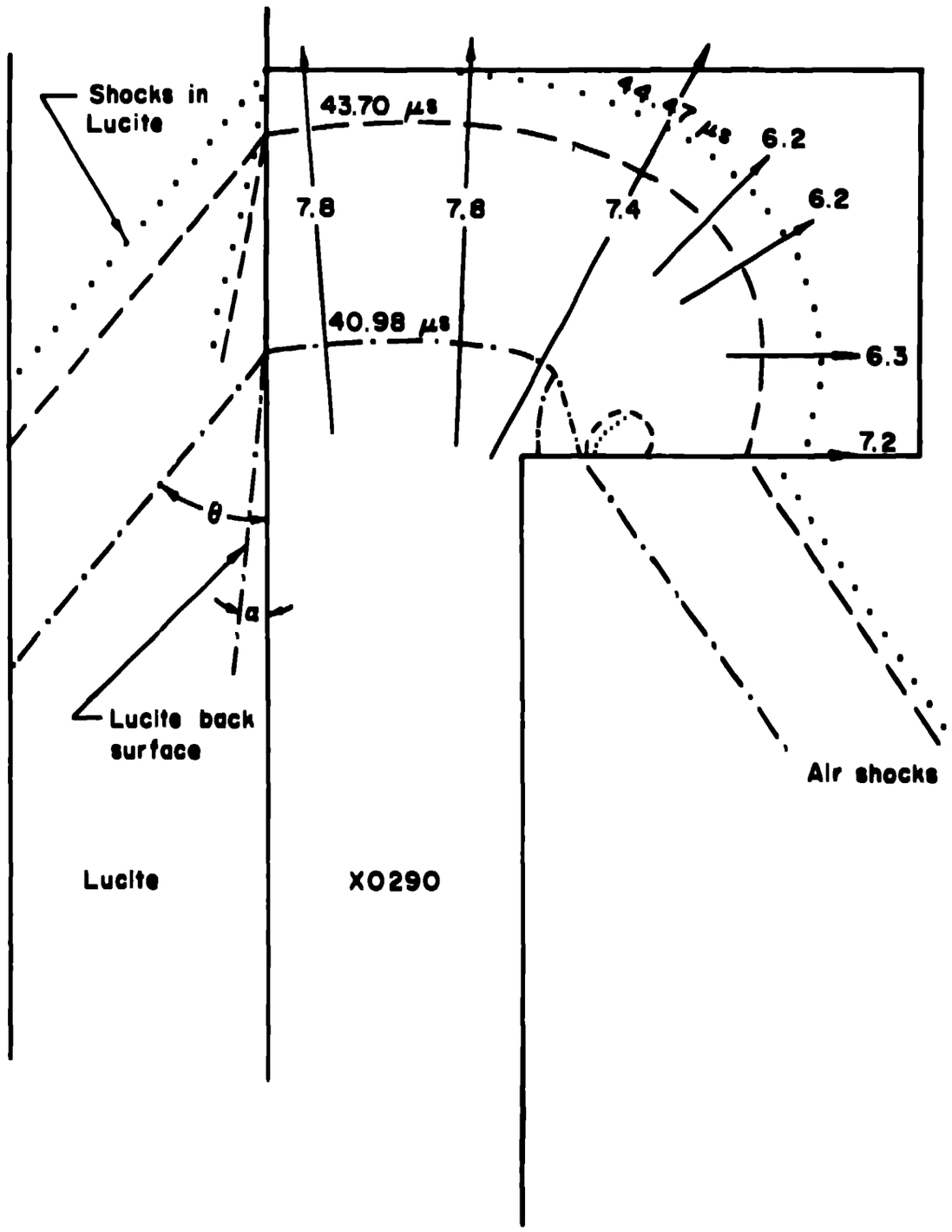
Shocks in Lucite
43.70 μs
44.47 μs
6.2
6.2
7.8
7.8
7.4
40.98 μs
6.3
7.2
θ
α
Lucite back surface
Air shocks
Lucite
XO290

Fig. 35

COMPARISON OF HE CHARACTERISTICS

HE	ρ_o (g/cm^3)	γ	P_{CJ} (GPa)	P_{LUCITE} (GPa)	Area[a] (cm^2)
X-0219	1.914	2.4	31.7	11.3	1.20
9502	1.892	2.4	32.9	11.8	0.12
9501	1.767	2.9	33.8	11.2	0
TNT	1.637	3.2	18.9	—	—
Comp B	1.713	2.8	29.2	10.5	—

[a]Area of unreacted zone at the corner

Fig. 36

RESULTS FROM CORNER TURNING

- A zone of unreacted explosive is present at the corner for insensitive explosives but not for 9501
- Zone size and shape nearly constant but very much smaller for 9502 than X-0219
- Zone completely enveloped by HE products at later times
- Reduction in detonation pressure at corner
- Calculated detonation pressure and γ - value nearly equal for X-0219 and 9502

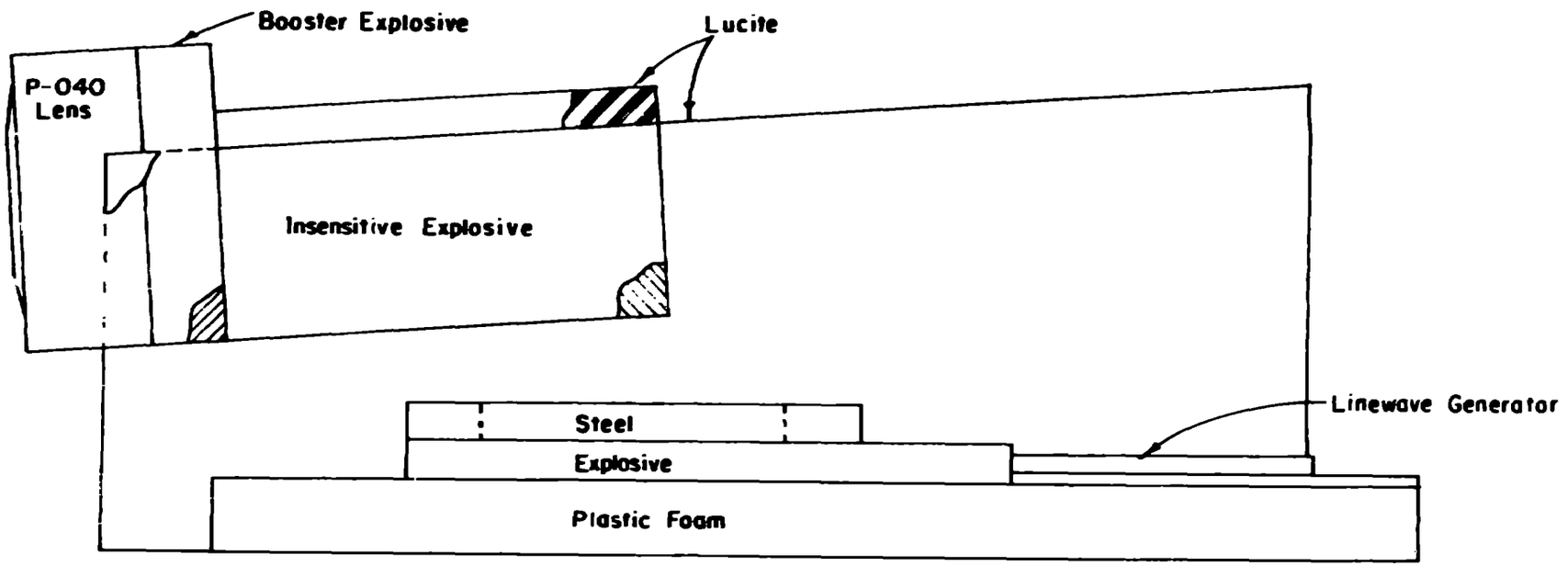
Booster Explosive
Lucite
P-040
Lens
Insensitive Explosive
Linewave Generator
Steel
Explosive
Plastic Foam

Fig. 38

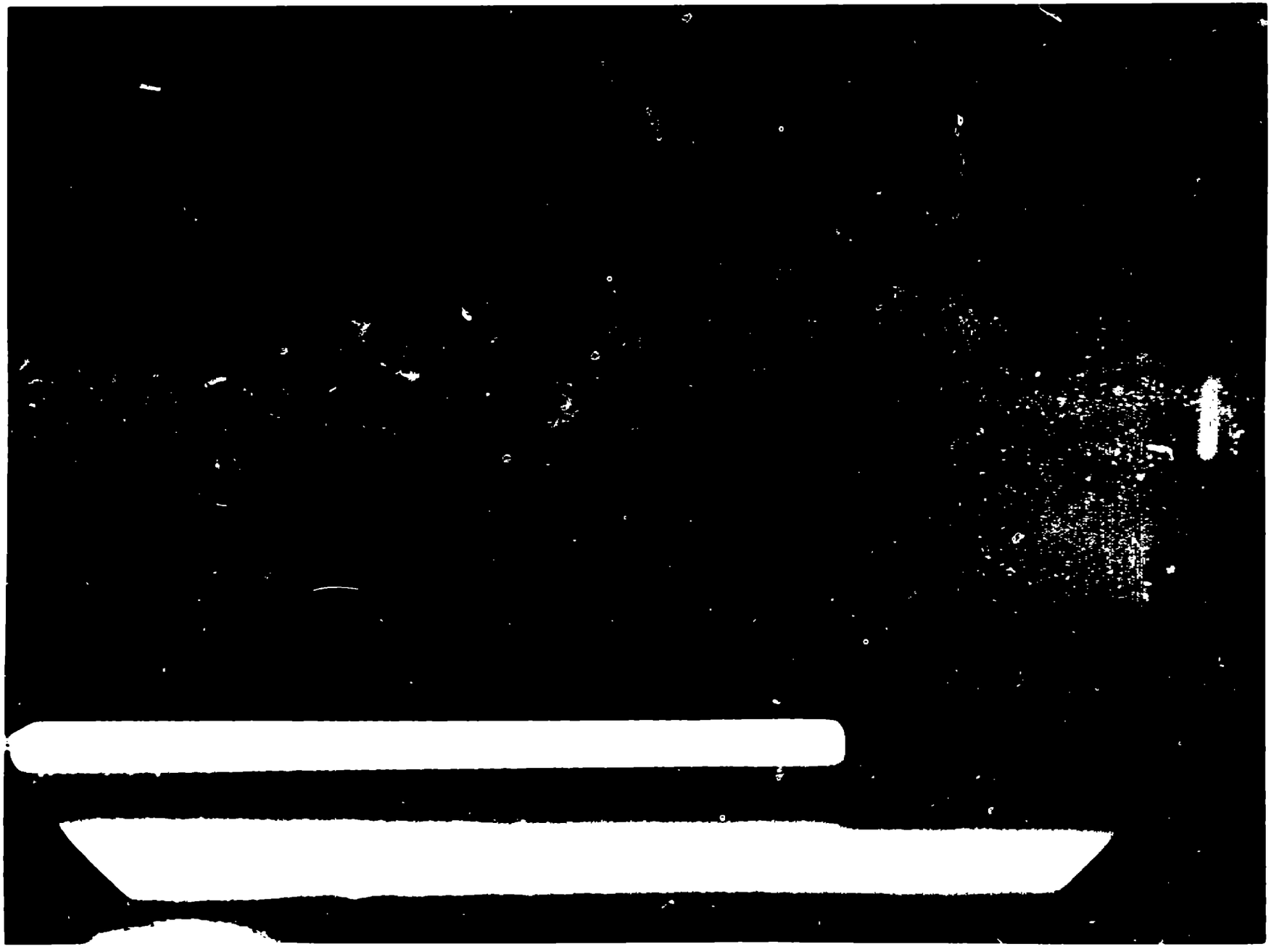

Fig. 39

Fig. 40

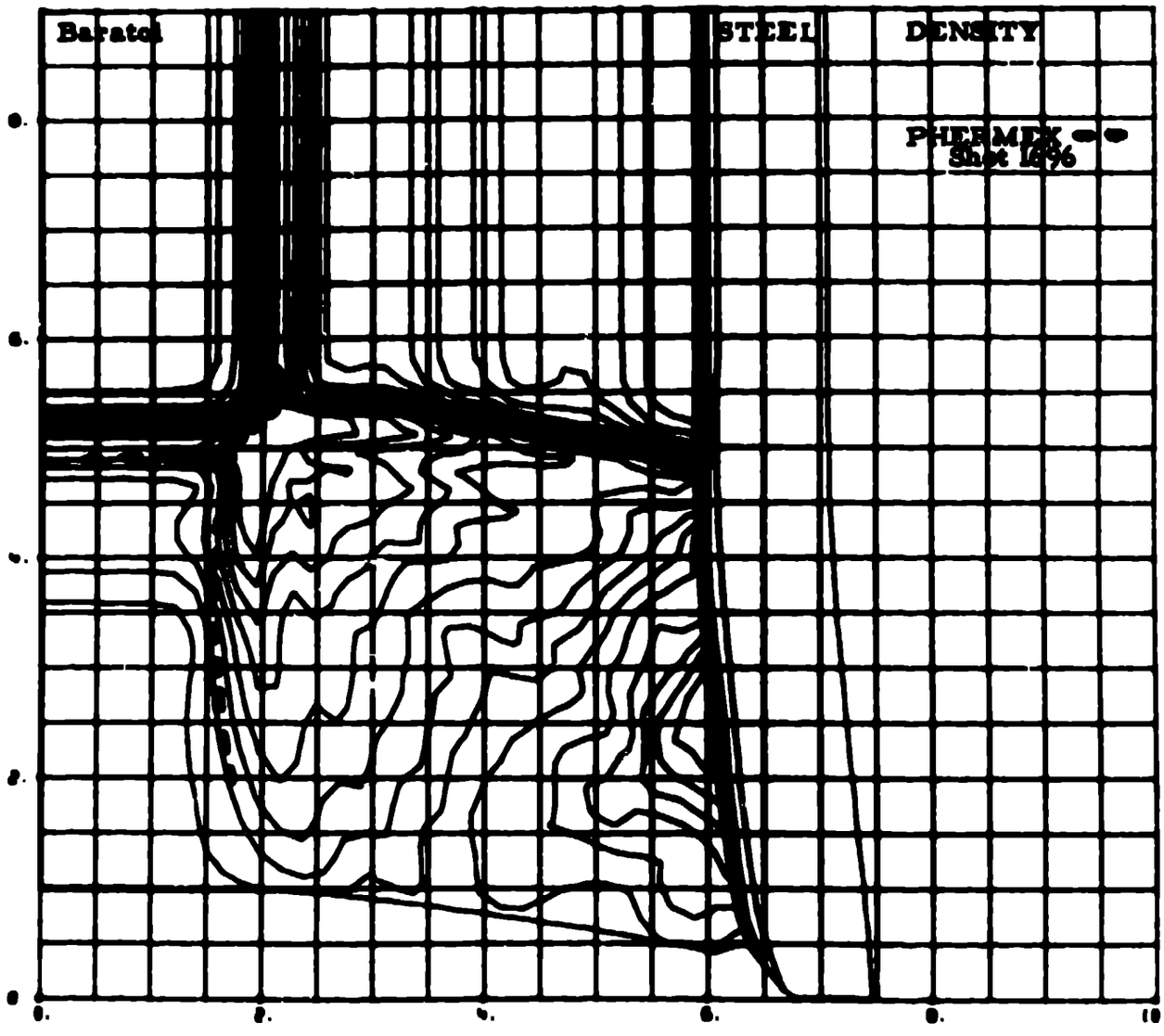

Fig. 41

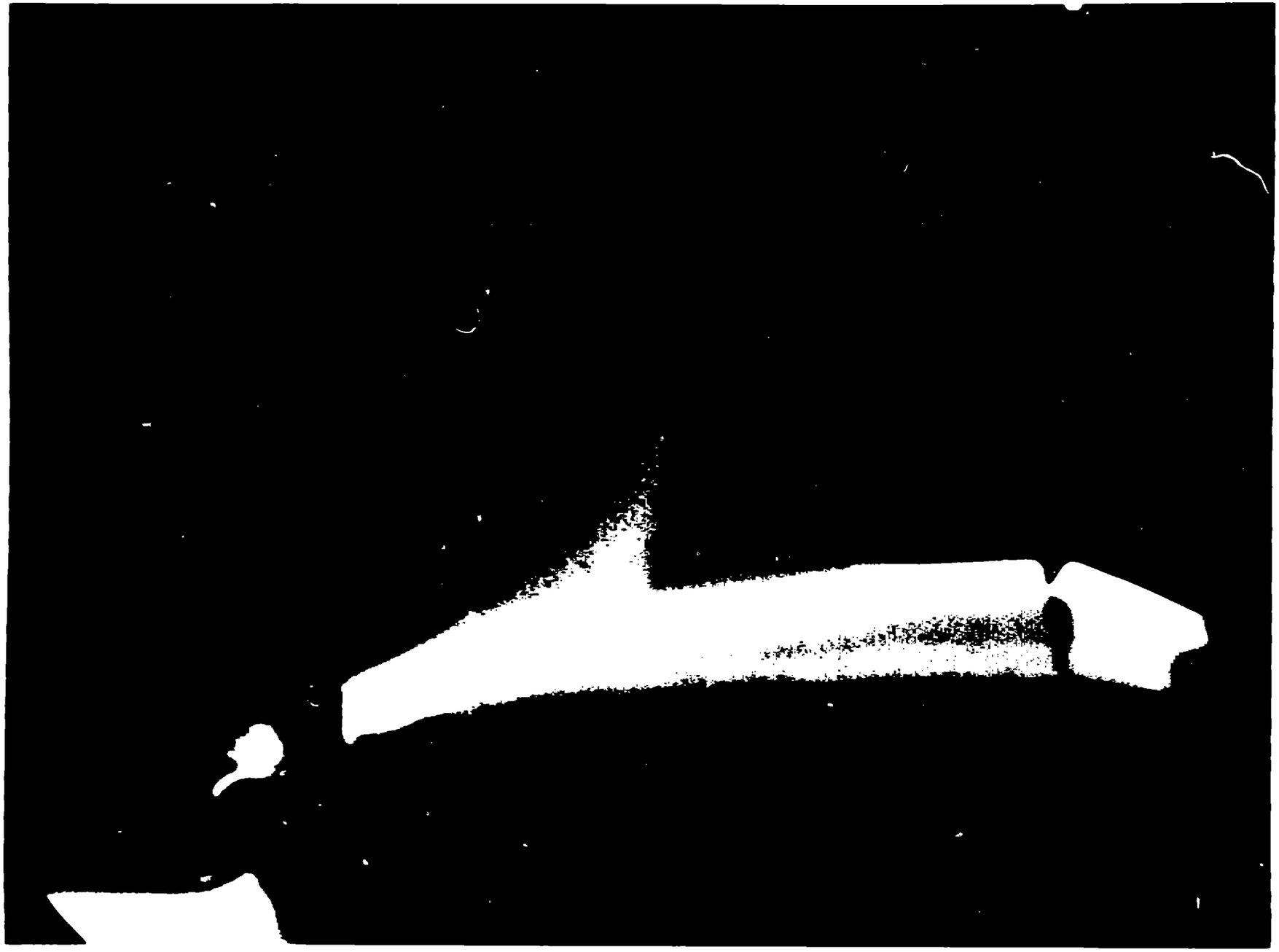

Fig. 42

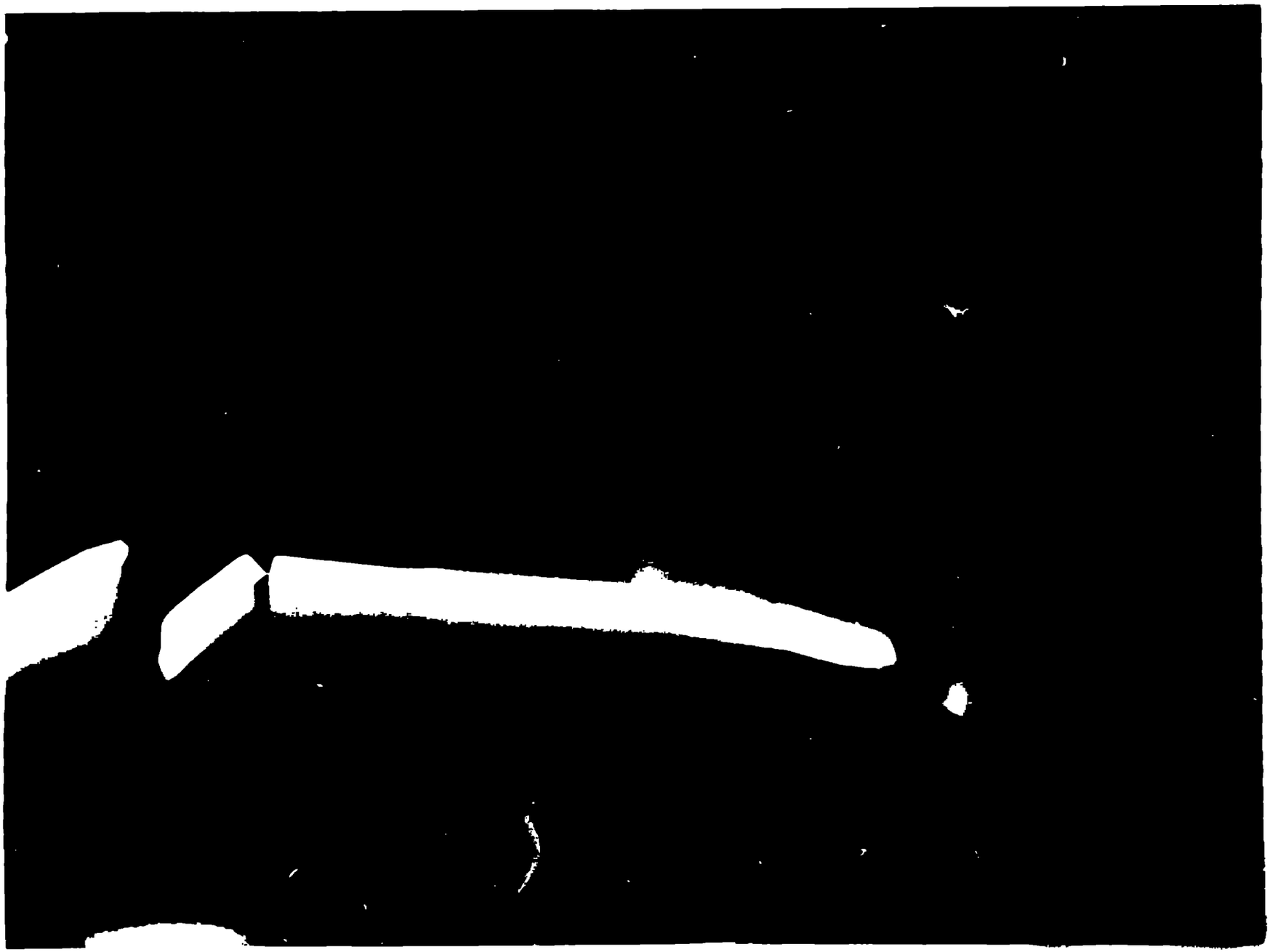

Fig. 43

Fig. 44

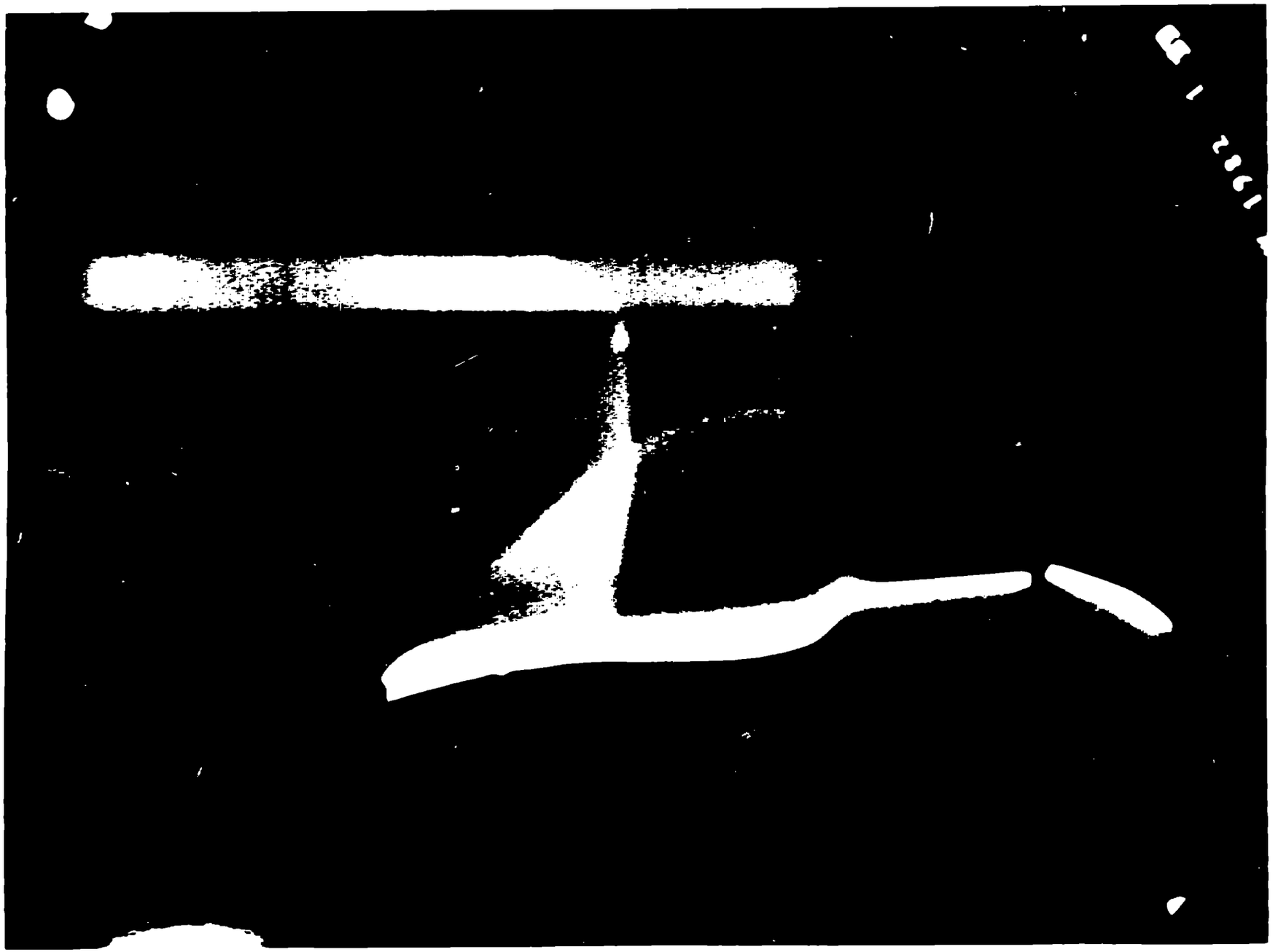

Fig. 45

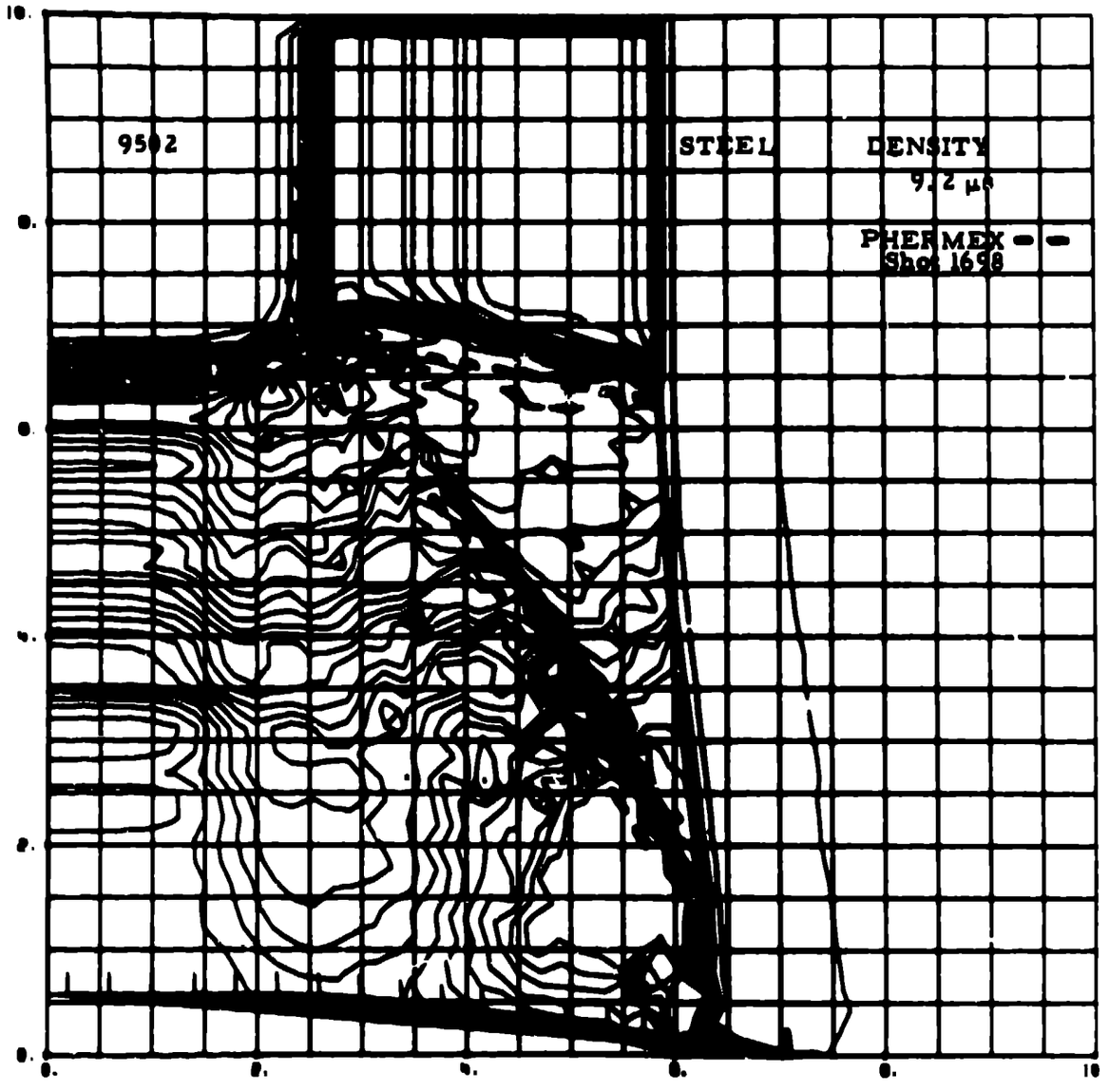

Fig. 46

RESULTS OF PRESHOCKED EXPLOSIVE STUDIES

- The detonation wave in X-0219 was quenched as it propagated into a region of the explosive precompressed by a shock wave of 6.0 GPa.

- The detonation wave in 9502 was quenched when propagating into a region of the explosive precompressed by shock pressures of 2.5 and 6.0 GPa.

- No change in the character of the detonation wave in 9502 as it propagated into a region of the explosive in which a 14.0 GPa shock wave had transformed to a detonation wave.